AD-A220 366

NUSC Technical Report 8599
15 October 1989

Estimation of Noise Field Directionality; Comparison with Fourier Series Method

Albert H. Nuttall
Surface ASW Directorate

DTIC
ELECTE
APR 12 1990
S D
D

Naval Underwater Systems Center
Newport, Rhode Island / New London, Connecticut

Approved for public release; distribution is unlimited.

90 04 12 017

Preface

This research was conducted under NUSC Project No. A75215, Subproject No. R00N000, "Determination of Concentrated Energy Distribution Functions in the Time-Frequency Plane," Principal Investigator Dr. Albert H. Nuttall (Code 304). This technical report was prepared with funds provided by the NUSC In-House Independent Research and Independent Exploratory Development Program, sponsored by the Office of Chief of Naval Research. Also, this work was sponsored by the NUSC Special Projects Office, Code 01Y, under Job Order No. 701Y12.

The technical reviewer for this report was James B. Donald (Code 01Y).

Reviewed and Approved: 15 October 1989

Daniel M. Viccione
Associate Technical Director
Research and Technology

REPORT DOCUMENTATION PAGE

Form Approved
OMB No. 0704-0188

Public reporting burden for this collection of information is estimated to average 1 hour per response, including the time for reviewing instructions, searching existing data sources, gathering and maintaining the data needed, and completing and reviewing the collection of information. Send comments regarding this burden estimate or any other aspect of this collection of information, including suggestions for reducing this burden, to Washington Headquarters Services, Directorate for Information Operations and Reports, 1215 Jefferson Davis Highway, Suite 1204, Arlington, VA 22202-4302, and to the Office of Management and Budget, Paperwork Reduction Project (0704-0188), Washington, DC 20503

1. AGENCY USE ONLY (Leave blank)	2. REPORT DATE	3. REPORT TYPE AND DATES COVERED
	15 OCT 1989	

4. TITLE AND SUBTITLE
ESTIMATION OF NOISE FIELD DIRECTIONALITY; COMPARISON WITH FOURIER SERIES METHOD

5. FUNDING NUMBERS
PR A75215
701Y12

6. AUTHOR(S)
Albert H. Nuttall

7. PERFORMING ORGANIZATION NAME(S) AND ADDRESS(ES)
Naval Underwater Systems Center
New London Laboratory
New London, CT 06320

8. PERFORMING ORGANIZATION REPORT NUMBER
TR 8599

9. SPONSORING/MONITORING AGENCY NAME(S) AND ADDRESS(ES)
Office of the Chief of Naval Research
Arlington, VA 22217-5000

10. SPONSORING/MONITORING AGENCY REPORT NUMBER

11. SUPPLEMENTARY NOTES

12a. DISTRIBUTION/AVAILABILITY STATEMENT
Approved for public release; distribution is unlimited.

12b. DISTRIBUTION CODE

13. ABSTRACT (Maximum 200 words)

For a line array immersed in a stationary homogeneous noise field, the noise field directionality, at any temporal-frequency of interest, is estimated without any a priori assumptions about the field and without the limitations of ill-conditioning. The key to this development is the deferment of the inherent discretization associated with an array until after the integral equation for the noise field directionality has been solved in terms of the observed spatial correlation.

Comparison with the Fourier series method reveals nearly identical results, except that the Fourier series method has some inaccurate low-order Fourier coefficients. Also, no Bessel function evaluations are required for the new method proposed here; instead, one FFT suffices for approximate evaluation of the field directionality. However, neither procedure has the superresolution capability of some of the recent eigen-decomposition approaches.

14. SUBJECT TERMS
Noise Field Directionality
Aliasing
Smoothing
Fourier Series Method
Fourier Integral Method;
Equispaced Line Arrays

15. NUMBER OF PAGES
62

16. PRICE CODE

17. SECURITY CLASSIFICATION OF REPORT	18. SECURITY CLASSIFICATION OF THIS PAGE	19. SECURITY CLASSIFICATION OF ABSTRACT	20. LIMITATION OF ABSTRACT
Unclassified	Unclassified	Unclassified	Unlimited

TABLE OF CONTENTS

LIST OF ILLUSTRATIONS

LIST OF TABLES

LIST OF SYMBOLS

θ	polar angle, figures 1 and 2
ϕ	azimuthal angle, figure 1
f	temporal-frequency
$N(f,\theta,\phi)$	noise field directionality at frequency f, (1)
M	number of receiving elements
G(f)	cross-spectral matrix of size MxM
$\tau_k(\theta,\phi)$	wavefront time delay to k-th element, (2)
$H_k(f,\theta,\phi)$	transfer function to k-th element, (2)
$G_{kj}(f)$	cross-spectrum between elements k and j, (4)
d_k	distance of k-th element from reference point, (5)
c	speed of propagation, (5)
$\bar{N}(f,\theta)$	integrated (averaged) directionality, (8)
d	element spacing, (9)
f_o	design frequency, (11),(12)
α	$\pi f/f_o$, (11)
u	bearing, $\cos\theta$, (11)
λ_o	design wavelength, c/f_o,(12)
C(p)	spatial correlation function, (13),(15)
B(u)	directionality function, (14)
δ	delta function, (18)
$B_b(u)$	approximation to B(u), (20)
$\circledast$	convolution, (21)
λ	wavelength, c/f, (21)
$B_c(u)$	approximation to B(u), (25)
w_n	weights used for approximate field, (25)

A-1

LIST OF SYMBOLS (cont'd)

$w(p)$	continuous weighting function, (27),figure 5
$W(u)$	window function, (30)
$B_a(u)$	approximation to B(u), (32)
K	size of discrete Fourier transform, (33)
Δ_x	sampling increment in x, (34),(59)
$A(\theta)$	noise field directionality, (37),(39)
a_q	Fourier series coefficient, (40)
$R(\theta)$	right-hand side of (40)
$J_q(x)$	Bessel function, (41)
sub r	real part, (43)
sub i	imaginary part, (44)
θ_o	plane-wave arrival angle, (49)
u_o	$\cos\theta_o$, (50)
$\tilde{a}_q$	approximate Fourier coefficient, (58)
q'	critical q value, (63)
L	length of array, (M-1)d, (64)
Δ_θ	resolution in θ, (65)

ESTIMATION OF NOISE FIELD DIRECTIONALITY; COMPARISON WITH FOURIER SERIES METHOD

INTRODUCTION

The possibility of estimating the directionality of a stationary homogeneous noise field, directly from the element outputs of a line array, was investigated in [1,2,3] and found feasible only for small array sizes, due to ill-conditioning of the solutions of the fundamental least-squares equations relating the observed discrete spatial correlations to the impingent field. In addition, the possibility of incorporating a priori information about the field directionality and allowing for additive uncorrelated noises at the elements were considered in [2].

Recently, the ill-conditioning associated with these approaches was circumvented in [4] by employing a Fourier series method for the unknown field. However, this method requires numerous Bessel function evaluations and can have inaccurate low-order expansion coefficients, leading to bias in the estimated field directionality. Here, we will eliminate both of these drawbacks.

NOISE FIELD CHARACTERIZATION

Consider a (wide-sense) stationary homogeneous noise field characterized by directionality $N(f,\theta,\phi)$ that measures the power density spectrum at temporal-frequency f, due to noise arrivals from direction (θ,ϕ). See figure 1. This characterization presumes that noise arrivals from different directions are uncorrelated and thereby precludes multipath arrivals, for example.

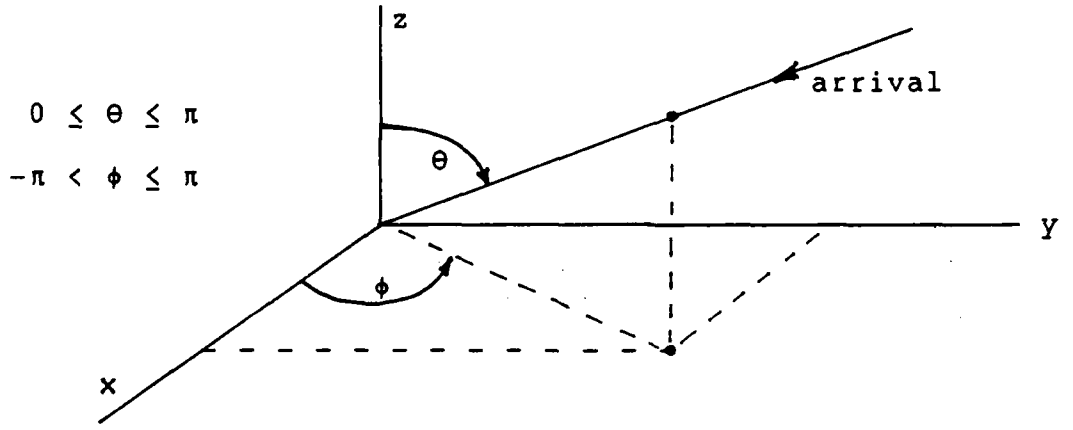

Figure 1. Angular Geometry

Suppose a collection of M receiving elements with arbitrary, but known, locations is immersed in this field. The largest amount of second-order information that can be extracted from these element outputs is the set of joint probability density functions between elements. However, in so far as estimating $N(f,\theta,\phi)$ is concerned, there is no need to retain anything more about the element outputs than the (Hermitian) matrix G(f) of their cross-spectral functions $G_{kj}(f)$, $1 \leq k,j \leq M$.

In order to relate $G_{kj}(f)$ to noise field directionality $N(f,\theta,\phi)$, consider the power density spectrum of the elemental contribution due to solid angle $d\theta\, d\phi\, \sin\theta$ centered at (θ,ϕ), namely

$$d\theta\, d\phi\, \sin\theta\, N(f,\theta,\phi). \tag{1}$$

In addition, let $\tau_k(\theta,\phi)$ be the time taken for a noise arrival from direction (θ,ϕ) to reach sensor k of a receiving array. Consequently, the transfer function applied to this arrival in reaching the k-th sensor is

$$\exp[-i2\pi f\tau_k(\theta,\phi)] \equiv H_k(f,\theta,\phi). \tag{2}$$

Then the cross-spectrum of the outputs of omnidirectional sensors k and j, owing to the elemental contribution (1), is

$$d\theta\, d\phi\, \sin\theta\, N(f,\theta,\phi)\, H_k(f,\theta,\phi)\, H_j(f,\theta,\phi)^* =$$

$$= d\theta\, d\phi\, \sin\theta\, N(f,\theta,\phi)\, \exp[-i2\pi f\{\tau_k(\theta,\phi)-\tau_j(\theta,\phi)\}]. \tag{3}$$

Assuming that the noise arrivals from different directions are uncorrelated, the cross-spectrum $G_{kj}(f)$ of the outputs of sensors k and j is given by the sum of components (3) over all angular space:

$$G_{kj}(f) = \int_0^{\pi} d\theta \int_{-\pi}^{\pi} d\phi\, \sin\theta\, N(f,\theta,\phi)\, \exp[-i2\pi f\{\tau_k(\theta,\phi)-\tau_j(\theta,\phi)\}]. \tag{4}$$

This result holds for $1 \le k,j \le M$, where M is the number of sensors in the receiving array. $N(f,\theta,\phi)$ is called the noise field directionality at temporal-frequency f. The product

$\sin\theta\, N(f,\theta,\phi)$ could be called the plane-wave density.

Equation (4), for all k,j, constitutes the totality of information about $N(f,\theta,\phi)$ from the available elements. The problem is to estimate $N(f,\theta,\phi)$ from measurements of $\{G_{kj}(f)\}$. It should be noted that not all $\{G_{kj}(f)\}$ contain independent information. Thus, $G_{kk}(f) = G_{11}(f)$ for all k, and $G_{kj}(f) = G^{*}_{jk}(f)$ for all k,j. Also, for example, if elements 1,2 and 3,4 have $\tau_1-\tau_2 = \tau_3-\tau_4$ for all θ,ϕ, (4) indicates that $G_{12}(f) = G_{34}(f)$; this is due to the homogeneity of the noise field.

Array processing techniques, whether they are standard delay and add, weighted, or optimum (adaptive), result in a preprocessing of noise field directionality $N(f,\theta,\phi)$. Attempts to then estimate $N(f,\theta,\phi)$ from these processed quantities must, in some sense, undo what the array processing has already done. But why should array processing be used on the elements at all, when we are interested in estimating the noise field directionality? An "optimum" estimation technique should accept matrix G(f) as its input and emit an estimate of $N(f,\theta,\phi)$ as its output. This is the goal of this investigation.

LINE ARRAY

In this report, we will address only the case where the receiving array lies entirely on a single line in space. In figure 1, let θ be measured with respect to the location of the line. That is, let the line array lie along the $\theta = 0$ axis, namely the z-axis. See figure 2. Then if d_k is the distance (measured downward) of the k-th element from some reference point on the line, we have delay

$$\tau_k(\theta,\phi) = \frac{d_k}{c} \cos\theta \quad \text{for } 1 \leq k \leq M. \tag{5}$$

The values $\theta = 0$ and π correspond to endfire of the line array, and c is the speed of propagation.

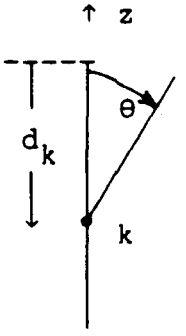

Figure 2. Geometry of Line Array

INTEGRATED DIRECTIONALITY FUNCTION

It follows from (4) and (5) that cross-spectrum

$$G_{kj}(f) = \int_0^{\pi} d\theta \int_{-\pi}^{\pi} d\phi \, \sin\theta \, N(f,\theta,\phi) \exp\left[-i2\pi f \frac{d_k - d_j}{c} \cos\theta\right] = \quad (6)$$

$$= \int_0^{\pi} d\theta \, \sin\theta \exp\left[-i2\pi f \frac{d_k - d_j}{c} \cos\theta\right] \bar{N}(f,\theta) \quad \text{for } 1 \le k,j \le M, \quad (7)$$

where we define integrated (or collapsed or averaged) noise directionality

$$\bar{N}(f,\theta) = \int_{-\pi}^{\pi} d\phi \, N(f,\theta,\phi). \quad (8)$$

Notice that $N(f,\theta,\phi)$ is defined in terms of a coordinate system centered on the line. According to (7), the only quantity that can be estimated about the noise field directionality is the integrated function $\bar{N}(f,\theta)$ in (8); this is a manifestation of the inherent conical symmetry of a line array response. The problem is to invert the measurements $\{G_{kj}(f)\}$ in (7) and solve for the quantity $\bar{N}(f,\theta)$, if possible.

EQUISPACED LINE ARRAY

For an equispaced line array, figure 2 can be specialized to

$$d_k = k\,d \qquad \text{for } 1 \le k \le M, \tag{9}$$

where d is the element spacing. Then, (7) becomes

$$G_{kj}(f) = \int_0^{\pi} d\theta\, \sin\theta\, \exp\left[-i\alpha(k-j)\,\cos\theta\right]\, \bar{N}(f,\theta) =$$

$$= \int_{-1}^{1} du\, \exp\left[-i\alpha(k-j)u\right]\, \bar{N}(f,\ \mathrm{acos}(u)), \tag{10}$$

where acos is the principal value inverse cosine function and

$$\alpha = \pi\,\frac{f}{f_o}, \qquad f_o = \frac{c}{2d}, \qquad u = \cos\theta. \tag{11}$$

The quantity f_o is the (design) frequency at which spacing d would be a half-wavelength:

$$\lambda_o = \frac{c}{f_o} = 2\,d. \tag{12}$$

Also, $u = 0$ corresponds to broadside of the line array.

At this point, a change of notation is very convenient. We suppress the explicit appearance of frequency f (it still appears through α in (11)) and express (10) as a spatial correlation

$$C(k-j) = \int_{-1}^{1} du\, \exp(-i\alpha(k-j)u)\, B(u), \tag{13}$$

where we recognize that the only dependence on k,j is through their difference and define the noise directionality function

$$B(u) = \left\{ \begin{array}{ll} \bar{N}(f, \text{acos}(u)) & \text{for } -1 < u < 1 \\ 0 & \text{for } |u| > 1 \end{array} \right\}. \qquad (14)$$

Finally, we modify spatial correlation (13) to

$$C(p) = \int_{-1}^{1} du \, \exp(-i\alpha p u) \, B(u). \qquad (15)$$

This can be considered as an integral equation for noise field directionality B(u), where α is known, and spatial correlation $C(p) = C^{*}(-p)$ is available only for integer p satisfying $|p| < M$; this was the approach considered in [1; section 2.3].

FOURIER INTEGRAL METHOD

Suppose that spatial correlation C(p) in (15) were available for all continuous p, not just the integers $|p| < M$. Then multiplying (15) by $\exp(i\alpha pu')$ and integrating over all p, we have, using (11),

$$\int_{-\infty}^{+\infty} dp\ \exp(i\alpha pu')\ C(p) = \int_{-\infty}^{+\infty} dp\ \exp(i\alpha pu') \int_{-1}^{1} du\ \exp(-i\alpha pu)\ B(u) =$$

$$= \int_{-1}^{1} du\ B(u)\ \frac{2\pi}{\alpha}\ \delta(u-u') = \left\{ \begin{array}{ll} \frac{2f_o}{f}\ B(u') & \text{if } -1 < u' < 1 \\ 0 & \text{otherwise} \end{array} \right\}. \quad (16)$$

That is,

$$B(u) = \frac{f}{2f_o} \int_{-\infty}^{+\infty} dp\ \exp(i\alpha up)\ C(p) \qquad \text{for } -1 < u < 1. \quad (17)$$

This is an explicit integral relationship for the (integrated) noise field directionality B(u) at bearing u, in terms of spatial correlation C(p) at separation p. We will call this the Fourier integral method for the determination of the noise field directionality.

As an example, if the field is composed of a single plane-wave arrival,

$$B(u) = \delta(u-u_o), \quad |u_o| < 1, \quad (18)$$

then (15) gives spatial correlation

$$C(p) = \exp(-i\alpha p u_o) \quad \text{for all } p, \tag{19}$$

and (17) restores directionality (18). We should also note that the highest rate of variation of spatial correlation C(p) is $\exp(\pm i\alpha p)$, obtained when $u_o \rightarrow \pm 1$. If we insert a higher variation for C(p) into solution (17), such as (19) with $|u_o| > 1$, we get nonzero values for directionality B(u) outside the allowed (-1,1) range of u, namely $\delta(u-u_o)$. Since this is disallowed according to (14), noisy estimates of spatial correlation C(p) require some preprocessing prior to insertion into (17); alternatively, nonzero values of B(u) for $|u| > 1$ might be ignored, but this is not an attractive approach.

INFINITELY-LONG DISCRETE ARRAY

Equation (17) gives the impression that spatial correlation C(p) is required for all continuous p. But since (13) indicates that C(p) will only be available for integer p, we consider that case first; in fact, we consider spatial correlation C(p) to be known for all integer p, which corresponds physically to an infinitely-long equispaced line array. The corresponding trapezoidal approximation to integral (17) for the noise field directionality is denoted as

$$B_b(u) = \frac{f}{2f_o} \sum_{n=-\infty}^{+\infty} \exp(i\alpha u n)\, C(n) \qquad \text{for all } u. \tag{20}$$

But this can be developed according to

$$B_b(u) = \frac{f}{2f_o} \int_{-\infty}^{+\infty} dp\, \exp(i\alpha u p)\, C(p) \sum_{n=-\infty}^{+\infty} \delta(p-n) =$$

$$= B(u) \circledast \sum_{n=-\infty}^{+\infty} \delta\left(u - n\,\frac{2\pi}{\alpha}\right) = \sum_{n=-\infty}^{+\infty} B\left(u - n\,\frac{2\pi}{\alpha}\right) =$$

$$= \sum_{n=-\infty}^{+\infty} B\left(u - n\,\frac{2f_o}{f}\right) \qquad \text{for all } u, \tag{21}$$

where $\circledast$ denotes convolution, and we used (11). Function $B_b(u)$ has period $2f_o/f$ in u; if we define $\lambda = c/f$, this period is λ/d, where we used (12).

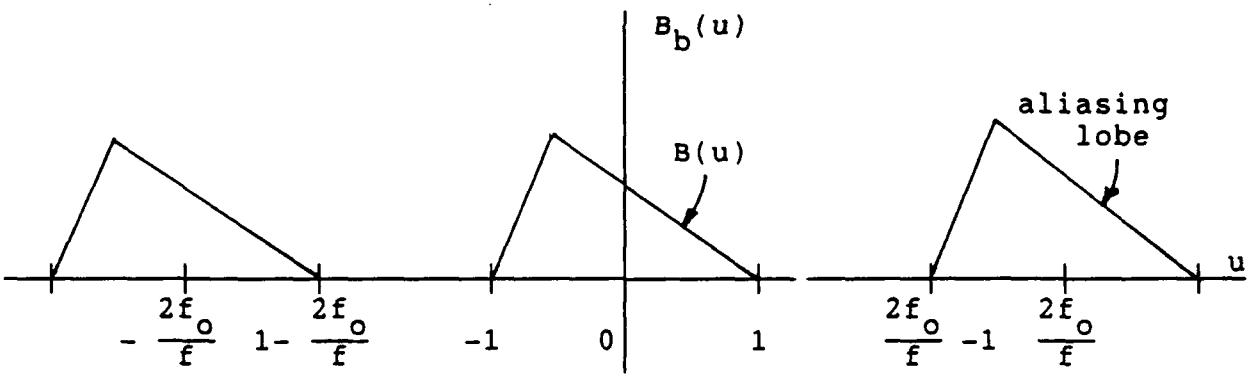

Figure 3. Approximation $B_b(u)$

The plot of approximation $B_b(u)$ to the noise field directionality in figure 3 reveals aliasing lobes separated by $2f_o/f$ on the u-axis. If $f < f_o$, that is, if the array is being used below its design frequency, then these lobes do not overlap, and we have

$$B_b(u) = B(u) \quad \text{for } -1 < u < 1. \tag{22}$$

Thus, exact recovery of the noise field directionality B(u) is possible from knowledge of spatial correlation C(p) at integer p, provided that

$$f < f_o, \quad \text{that is, } d < \lambda/2; \tag{23}$$

here, we used $\lambda = c/f$ and (12). The element spacing must be less than a half-wavelength at the temporal-frequency f of interest in order to avoid aliasing. The discrete nature of the array does not, in itself, prevent recovery of the field; it is the finite length of a physical array that causes problems.

If spatial correlation C(p) contains a component with too high a rate of variation, as, for example, (19) again with $|u_o| > 1$, we get $B(u) = \delta(u-u_o)$ as before. However, a plot of the corresponding $B_b(u)$ in figure 4 (for $u_o > 1$) reveals an aliased component within the fundamental range (-1,1). We would be led to believe that the noise field directionality has a component

$$\delta(u - u_1) = \delta\left(u - u_o + \frac{2f_o}{f}\right) , \tag{24}$$

which is incorrect. Thus, the discrete nature of an array can be a problem if the measured spatial correlation C(p) contains disallowed components, which show up as aliased components inside the fundamental range (-1,1) of u. This problem exists even if the array has infinite length.

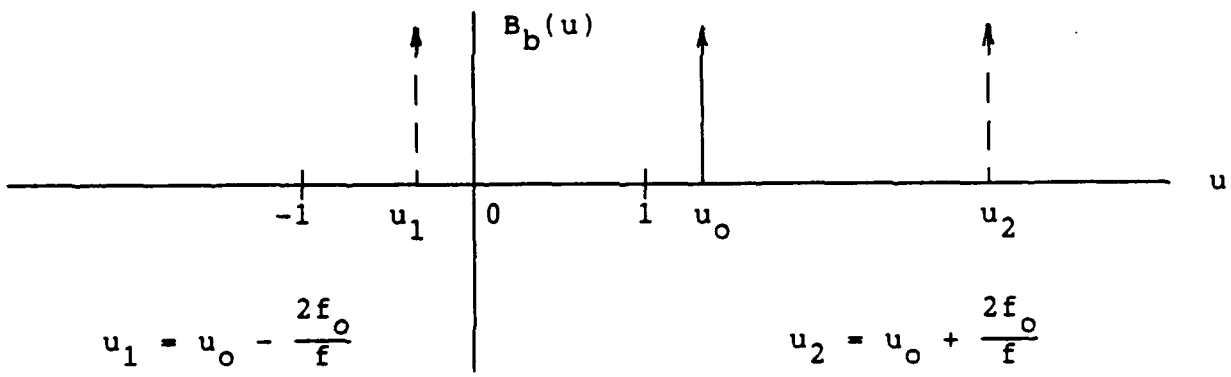

Figure 4. Aliasing of Disallowed Component

FINITE-LENGTH DISCRETE ARRAY

The approximate noise field directionality for a finite array of M elements is a modification of (20):

$$B_c(u) = \frac{f}{2f_o} \sum_{n=-\infty}^{+\infty} \exp(i\alpha u n)\, C(n)\, w_n \quad \text{for all } u, \tag{25}$$

where weights

$$w_n = 0 \quad \text{for } |n| \geq M. \tag{26}$$

We consider that weights $\{w_n\}$ are samples of a continuous function w(p); that is,

$$w_n = w(n), \tag{27}$$

where function w satisfies

$$w(p) = 0 \quad \text{for } |p| \geq M. \tag{28}$$

See figure 5. It then follows immediately from (25) and (20) that

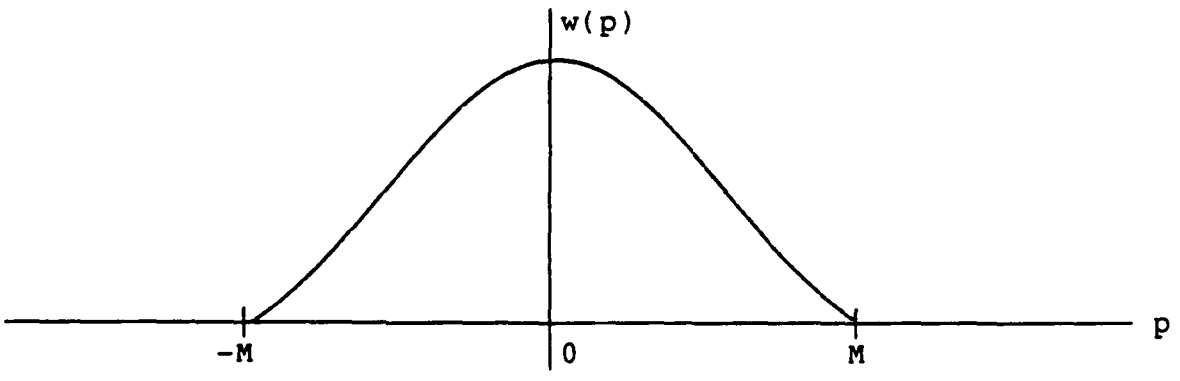

Figure 5. Weighting Function w(p)

$$B_c(u) = B_b(u) \circledast W(u), \tag{29}$$

where window

$$W(u) = \frac{f}{2f_o} \int_{-\infty}^{+\infty} dp \, \exp(i\alpha up) \, w(p). \tag{30}$$

(For the case of no weighting, that is, $w(p) = 1$ for all p, then $W(u) = \delta(u)$, and (29) reduces to (21).) The window W(u) has

$$\text{effective width} \quad \frac{1}{M} \frac{2f_o}{f} \quad \text{in u.} \tag{31}$$

(For flat weighting, that is, $w(p) = 1$ for $|p| < M$, the effective width is half of (31); however, the sidelobes of W(u) are then significant.)

Although the aliasing of $B_b(u)$ in figure 3 can be controlled through satisfaction of (23), the convolution result in (29) reveals that the true noise field directionality B(u) will be smeared by window W(u). This is a result of the finite length, (26), of the array. Also, (29) and (31) reveal that approximation $B_c(u)$ has no superresolution capabilities; in fact, the smaller that f is chosen below design frequency f_o, the more smeared $B_c(u)$ becomes. Thus, there is good reason to operate near the design frequency, that is, maximize f/f_o, in order to minimize the width in (31); however, there is the conflicting requirement depicted in figure 3 and (29), which points to smaller values of f/f_o. A compromise is in order.

If spatial correlation C(p) contains a disallowed component such as (19) with $|u_o| > 1$, (29) and figure 4 indicate the presence of a smeared and aliased component within the fundamental range (-1,1). Thus, such disallowed components should be preprocessed out of spatial correlation C(p) before submission into approximation (25).

APPROXIMATE FIELD

The approximate noise field directionality that we will consider at length, here, is obtained by setting $w_n = 1$ for $|n| < M$ in (25):

$$B_a(u) = \frac{f}{2f_o} \sum_{n=1-M}^{M-1} \exp(i\alpha u n)\, C(n) \quad \text{for} \quad -1 < u < 1. \qquad (32)$$

This is a sampled box-car approximation to the exact integral result for B(u) in (17). $B_a(u)$ has period $2f_o/f$ in u. If $|C(n)|$ for $|n| \geq M$ is substantially smaller than C(0), (32) could give a good approximation to B(u). If not, then one of the super-resolution techniques, such as maximum entropy, could be used to effectively extrapolate spatial correlation C(n) out to $n = \pm\infty$ and the transform carried out analytically in closed form.

Approximations (32) and (25) have the same form as [1; (41) and (42)], if weighting $\hat{w}(f,u)$ there is independent of u. Also, if $f = f_o$, (32) reduces identically to [1; (47) or (51)].

However, we do not solve any ill-conditioned equations here, when $f < f_o$; on the other hand, we have not minimized any error measure either.

The actual numerical evaluation of approximation $B_a(u)$ is best done by specializing to the particular argument values

$$B_a\left(\frac{k}{K}\,\frac{2f_o}{f}\right) = \frac{f}{2f_o} \sum_{n=1-M}^{M-1} \exp(i2\pi kn/K)\; C(n) =$$

$$= \frac{f}{2f_o}\left[C(0) + 2\;\mathrm{Re}\left\{\sum_{n=1}^{M-1} \exp(-i2\pi kn/K)\; C^*(n)\right\}\right], \qquad (33)$$

which can be accomplished by a discrete Fourier transform. The K values of k, that are swept out, cover an interval of length $2f_o/f$ in u, which is broader than the length 2 interval required, when $f < f_o$. See figure 3.

The exp(ix) function in (32) is being sampled at increment

$$\Delta_x = \alpha\, u = \pi\, \frac{f}{f_o}\, u\ . \qquad (34)$$

So, if $f < f_o$ and $|u| < 1$, then $|\Delta_x| < \pi$, meaning that exp(ix) has at least two samples per period. This is well known to be the requirement for avoidance of overlapped aliasing lobes and is corroborated by figure 3. This sampling rate interpretation will be very important later when we discuss the Fourier series method [4].

Similarly, the spatial correlation C(p) in (17) is being sampled at increment $\Delta_p = 1$. But since the sampling increment of exp(-ix) in (19), for basic elemental example (18), is

$$\Delta_x = \alpha u_o = \pi \frac{f}{f_o} u_o , \qquad (35)$$

we again have $|\Delta_x| < \pi$ if $f < f_o$ and $|u_o| < 1$. Thus, at least two samples per period are taken of spatial correlation C(p), as well, even if values of u_o near ± 1 occur.

DISCUSSION

It can be seen from (34) and (35) that the most troublesome cases will be when frequency f is near f_o and u_o is near ± 1, that is, when the array is employed at its design frequency and when arrivals come in near endfire. Since arrivals come in of their own accord, no control is had of u_o, except to turn the line array. And although one could choose $f < f_o$ in order to alleviate aliasing, losses in resolution will then occur, as (31) indicates. Thus, a trade-off is in order in regards to choice of f/f_o; perhaps, values somewhat less than 1 are a reasonable compromise, as was done in [1; figures 3,4,5]. Of course, a larger number of elements, M, always helps in improving resolution, as shown by (31); this is now a viable alternative, since there is no ill-conditioning as there was in [1].

The reason that we have been able to circumvent the ill-conditioning is that we have deferred the inherent sampling of (15), with increment $\Delta_p = 1$, until after we solved the integral equation for noise field directionality B(u) in explicit form (17). So, instead of facing up to the discrete issue, as explicitly posed in (13), we have put it off as long as possible, and have then addressed it in the various forms (20), (25), and (32), which are reasonable approximations to the ideal continuous result (17). This procedure of temporarily ignoring the discrete sampling associated with a line array was first presented in [4; section 3] in connection with a cosine series expansion for the field distribution; this latter procedure is fully developed in the next section.

FOURIER SERIES METHOD

In order to derive this method, we return to a combination of (14) and (15):

$$C(p) = \int_{-1}^{1} du \, \exp(-i\alpha p u) \, \bar{N}(f, \, a\cos(u)) =$$

$$= \int_{0}^{\pi} d\theta \, \exp(-i\alpha p \, \cos\theta) \, \sin\theta \, \bar{N}(f,\theta) \; . \qquad (36)$$

This equation relates the measured spatial correlation C(p), at integer separations p, to the integrated noise field directionality $\bar{N}(f,\theta)$ (see(8)). We again suppress the f dependence and define plane-wave density

$$A(\theta) = \sin\theta \, \bar{N}(f,\theta) \quad \text{for} \quad 0 < \theta < \pi \; , \qquad (37)$$

to obtain

$$C(p) = \int_{0}^{\pi} d\theta \, \exp(-i\alpha p \, \cos\theta) \, A(\theta) \; . \qquad (38)$$

As in (15) et seq., spatial correlation C(p) is known only for integer p satisfying $|p| < M$. Function $A(\theta)$ is the unknown field function that must be estimated. It is related to the B function of the preceding section according to

$$A(\theta) = \sin\theta \, B(\cos\theta) \quad \text{for} \quad 0 < \theta < \pi \; . \qquad (39)$$

See (37) and (14).

FOURIER SERIES EXPANSION

We expand $A(\theta)$ in a cosine series according to

$$A(\theta) = \sum_{q=0}^{+\infty} a_q \cos(q\theta) \quad \text{for} \quad 0 < \theta < \pi \ . \tag{40}$$

This basis is a complete set on interval $(0,\pi)$. See [5; page 92]. If we substitute (40) into (38), and interchange operations, we get

$$C(p) = \sum_{q=0}^{+\infty} a_q \int_0^{\pi} d\theta \exp(-i\alpha p \cos\theta) \cos(q\theta) =$$

$$= \pi \sum_{q=0}^{+\infty} a_q (-i)^q J_q(\alpha p) \ , \tag{41}$$

where we used [6; 9.1.21]. As a special case,

$$C(0) = \pi a_o \ , \tag{42}$$

which allows explicit determination of a_o.

Equation (41) constitutes an infinite set of complex simultaneous linear equations for coefficients $\left(a_q\right)_0^{\infty}$. If we split this equation into its real and imaginary parts, we have

$$\frac{1}{\pi} C_r(p) = \sum_{\substack{q=0 \\ q \text{ even}}}^{+\infty} a_q (-i)^q J_q(\alpha p) = \sum_{k=0}^{+\infty} a_{2k} (-1)^k J_{2k}(\alpha p) , \quad (43)$$

$$\frac{1}{\pi} C_i(p) = \sum_{\substack{q=1 \\ q \text{ odd}}}^{+\infty} a_q (-i)^{q+1} J_q(\alpha p) = \sum_{k=1}^{+\infty} a_{2k-1} (-1)^k J_{2k-1}(\alpha p) . \quad (44)$$

We now have two infinite sets of real simultaneous linear equations, one for the even coefficients, the other for the odd coefficients, in cosine expansion (40).

Since spatial correlation C(p) in (38) is only known for a finite number of discrete p values, namely integer $|p| < M$, there is no hope of solving for the infinite number of unknowns $\{a_q\}$ in (43) and (44). What we shall do, for the time being, is to <u>ignore</u> this limitation and pretend that C(p) is known for all continuous $p \geq 0$. (Of course, C(p) is then also known for $p < 0$, according to $C(-p) = C^*(p)$ from (15), since field B(u) is real.) This procedure was first propounded for the line array in [4].

We multiply both sides of (43) by $J_{2m}(\alpha p)/p$ and integrate over p, to obtain

$$\frac{1}{\pi} \int_0^{+\infty} dp \, \frac{J_{2m}(\alpha p)}{p} C_r(p) = \sum_{k=0}^{+\infty} a_{2k} (-1)^k \int_0^{+\infty} dp \, \frac{J_{2m}(\alpha p)}{p} J_{2k}(\alpha p) =$$

$$= \frac{a_{2m} (-1)^m}{2(2m)} \quad \text{for} \quad m \geq 1 ; \quad (45)$$

here, we used [6; 11.4.6]. In a similar fashion, from (44),

$$\frac{1}{\pi}\int_0^{+\infty} dp\ \frac{J_{2m-1}(\alpha p)}{p}\ C_i(p) = \sum_{k=1}^{+\infty} a_{2k-1}\ (-1)^k \int_0^{+\infty} dp\ \frac{J_{2m-1}(\alpha p)}{p}\ J_{2k-1}(\alpha p)$$

$$= \frac{a_{2m-1}\ (-1)^m}{2(2m-1)} \quad \text{for} \quad m \geq 1\ . \tag{46}$$

Combining (42), (45), and (46), we have

$$a_o = \frac{1}{\pi}\ C(0) = \frac{1}{\pi}\ C_r(0)\ ,$$

$$\left.\begin{aligned} a_{2m} &= \frac{2}{\pi}\ (-1)^m\ 2m \int_0^{+\infty} dp\ \frac{J_{2m}(\alpha p)}{p}\ C_r(p) \\ a_{2m-1} &= \frac{2}{\pi}\ (-1)^m\ (2m-1) \int_0^{+\infty} dp\ \frac{J_{2m-1}(\alpha p)}{p}\ C_i(p) \end{aligned}\right\} \quad \text{for } m \geq 1. \tag{47}$$

Convergence of the first integral at $p = 0$ is guaranteed since $J_{2m}(\alpha p)/p \to 0$ as $p \to 0$, because $2m \geq 2$. The second integral also converges at $p = 0$, since $J_{2m-1}(\alpha p)\ C_i(p)/p \to 0$ as $p \to 0$, because $2m-1 \geq 1$ and $C_i(0) = 0$. Thus, both integrands in (47) approach zero at the origin.

We now have explicit integral relations for the coefficients $\{a_q\}$ in the cosine series expansion of $A(\theta)$ in (40). They are exact results for $\{a_q\}$, presuming that spatial correlation $C(p)$ is available for <u>all</u> <u>continuous</u> $p \geq 0$. They agree with [4; (13)-(15)].

EXAMPLE

Consider the same single plane-wave arrival given in (18):

$$B(u) = \delta(u - u_o) , \quad |u_o| < 1. \tag{48}$$

Then (39) yields

$$A(\theta) = \sin\theta\, \delta(\cos\theta - u_o) = \delta(\theta - \theta_o) \quad \text{for} \quad 0 < \theta < \pi , \tag{49}$$

where $\theta_o = \text{acos}(u_o)$, $0 < \theta_o < \pi$. Substitution in (38) gives spatial correlation

$$C(p) = \exp(-i\alpha p \cos\theta_o) = \exp(-i\alpha p u_o) , \tag{50}$$

as in (19). When this result is used in (47), the coefficients are found to be (see appendix A)

$$a_o = \frac{1}{\pi} ,$$

$$a_q = \frac{2}{\pi} \cos(q\, \theta_o) \quad \text{for } q \geq 1 , \tag{51}$$

<u>independent</u> of α. Then the summation on the right-hand side of (40) becomes (appendix A)

$$R(\theta) = \sum_{m=-\infty}^{+\infty} \left[\delta(\theta - \theta_o - m2\pi) + \delta(\theta + \theta_o - m2\pi)\right] \quad \text{for all } \theta. \tag{52}$$

The plot of this function in figure 6 reveals that the only impulse component lying in the allowed range of θ, namely $(0,\pi)$, is that at $\theta = \theta_o$. Therefore,

$$A(\theta) = \delta(\theta - \theta_o) \quad \text{for} \quad 0 < \theta < \pi \ , \tag{53}$$

as desired. Thus, the use of all the exact coefficients $\{a_q\}$ in (51) restores field distribution $A(\theta)$ precisely.

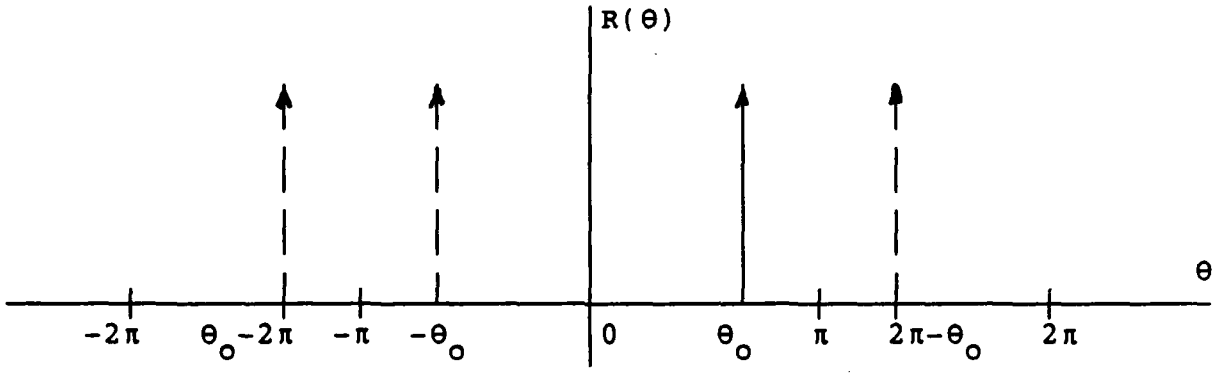

Figure 6. Summation $R(\theta)$ in (40)

DISALLOWED COMPONENT

The highest rate of variation of spatial correlation $C(p)$ in (50) is $\exp(\pm i\alpha p)$, just as in (19) et seq. If we insert a higher variation for $C(p)$ into integral solution (47) for the coefficients, namely

$$C(p) = \exp(-i\alpha p u_o) \ , \quad u_o > 1 \ , \tag{54}$$

we obtain [7; 6.693 1&2]

$$a_o = \frac{1}{\pi} ,$$

$$a_q = \frac{2}{\pi} Q^q \quad \text{for } q \geq 1 , \tag{55a}$$

where

$$Q = \frac{1}{u_o + \sqrt{u_o^2 - 1}} = u_o - \sqrt{u_o^2 - 1} , \tag{55b}$$

independent of α. Use of these coefficients in summation (40) gives reconstructed field (right-hand side of (40))

$$R(\theta) = \frac{1}{\pi} \frac{\sqrt{u_o^2 - 1}}{u_o - \cos\theta} . \tag{56}$$

A plot of this function in figure 7 reveals that it is spread out over the entire $(0,\pi)$ interval; this is in contrast to the Fourier integral method in (19) which correctly restored a zero field in the fundamental interval, namely

$$B(u) = \delta(u - u_o) , \quad u_o > 1 , \tag{57}$$

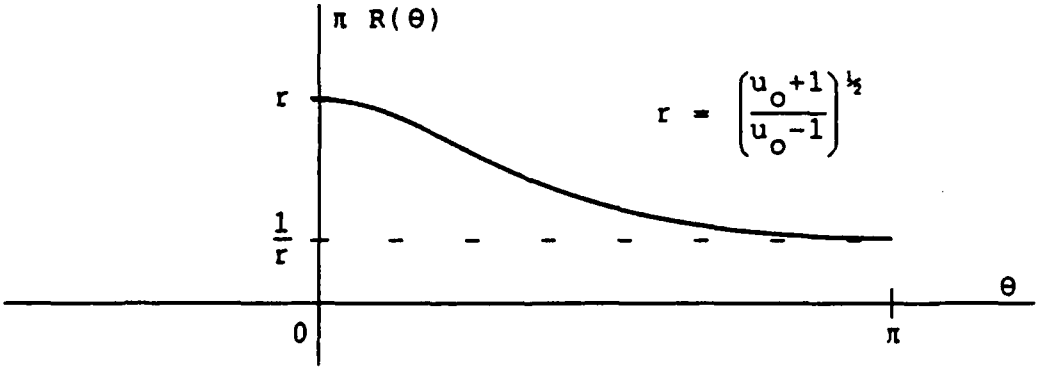

Figure 7. Reconstructed Field $R(\theta)$ for $u_o > 1$

for this example. Thus, the Fourier series method gives nonzero field values for $0 < \theta < \pi$, even when all the coefficients $\{a_q\}$ are determined exactly by the integrals in (47). The use of noisy estimates for C(p) in (47) is therefore more debilitating for the Fourier series method than for the Fourier integral method, and some preprocessing (that is, low-pass filtering) of the available spatial correlation C(p) values is required prior to insertion into (47). If this is not done, a spurious background will be yielded from the Fourier series method in the fundamental range $0 < \theta < \pi$, due to "spillover" from disallowed components of C(p).

Substitution of the reconstructed field $R(\theta)$ of (56) and figure 7 into the right-hand side of (38) does not restore the spatial correlation (54) for this example with $u_o > 1$. This is expected, since the coefficients $\{a_q\}$ in (55) decay with q, preventing summation (40) for $A(\theta)$ from retaining the arbitrarily narrow behavior required versus θ, namely the delta function in (49).

DISCRETE ARRAY

For an equispaced line array of M elements, (13) indicates that spatial correlation C(p) will be available only for integer $|p| < M$. We therefore adopt, as approximations to the exact integral results in (47), the forms

$$\left.\begin{aligned} \tilde{a}_{2m} &= \frac{2}{\pi}(-1)^m\, 2m \sum_{n=1}^{M-1} \frac{J_{2m}(\alpha n)}{n} C_r(n) \\ \tilde{a}_{2m-1} &= \frac{2}{\pi}(-1)^m\,(2m-1) \sum_{n=1}^{M-1} \frac{J_{2m-1}(\alpha n)}{n} C_i(n) \end{aligned}\right\} \quad \text{for } m \geq 1 , \tag{58}$$

along with $\tilde{a}_o = a_o = C_r(0)/\pi$; see [4; (16)-(18)]. These are explicit finite sums for the approximate coefficients $\{\tilde{a}_q\}$, to be used in the cosine series (40) in place of the exact, but unknown, $\{a_q\}$. (The terms for $n = 0$ in the summands of (58) are zero by virtue of the discussion under (47).)

Several potential problems exist with approximations (58). First, the increment in the $J_k(x)$ Bessel functions in (58) is

$$\Delta_x = \alpha = \pi \frac{f}{f_o} . \tag{59}$$

For the design frequency $f = f_o$, (that is, $d = \lambda/2$), this increment is π, which is rather large. The plots of $J_k(x)$ in figure 8, for $0 < x < 20\pi$ and selected k values between 1 and 35, reveal that the low-order Bessel functions are very poorly sampled at values $x_n = n\pi$, especially for small n. For example, the peaks

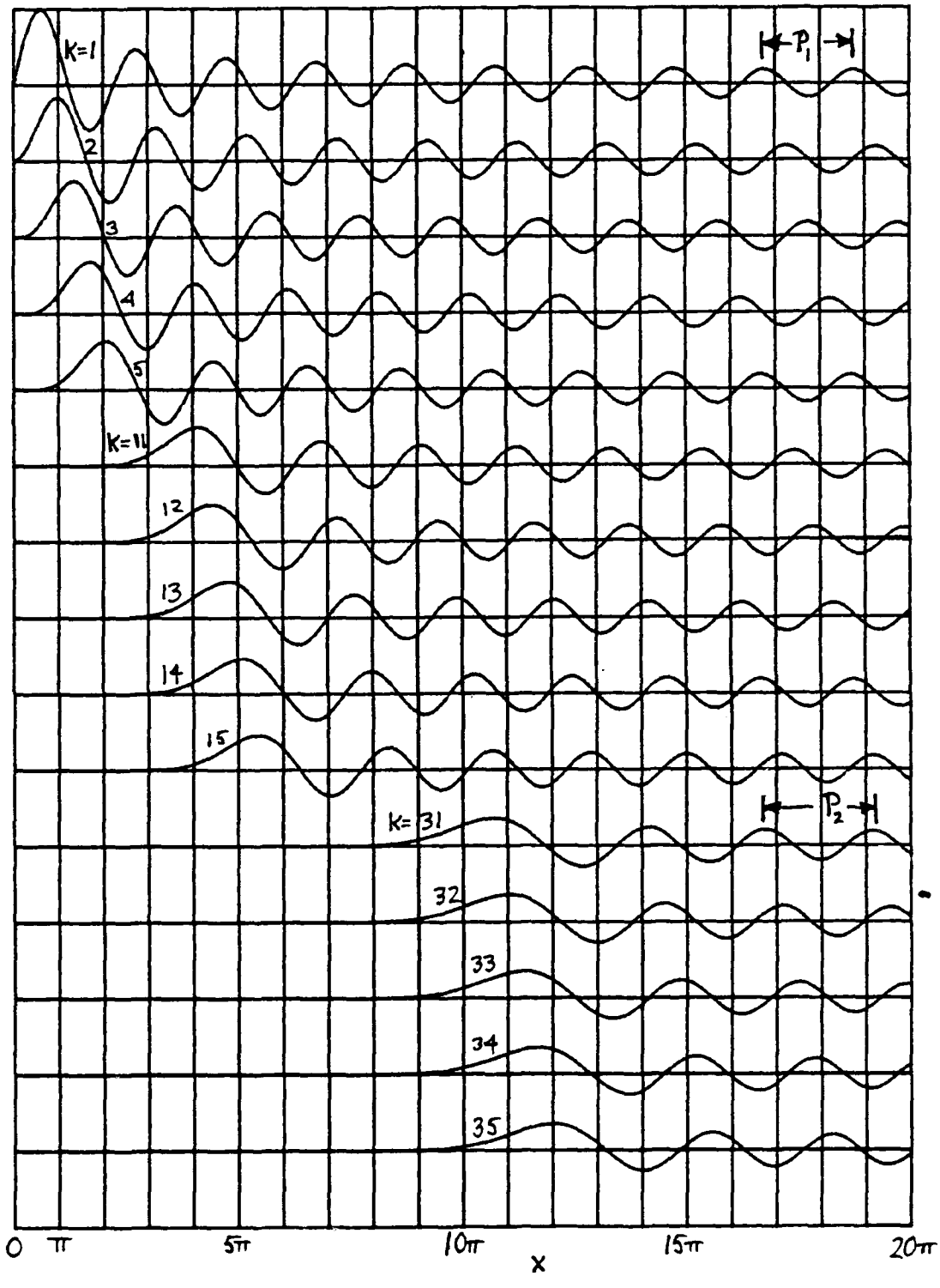

Figure 8. Bessel Functions $J_k(x)$

of $J_1(x)$ at x near .6π and 1.7π are badly represented by samples at $x = \pi$ and 2π. (The curves in figure 8 are scaled relative to the largest value of $J_1(x)$ at x near .6π.)

Of more relevance are the plots of weighted functions $J_k(x)/x$ in figure 9, because this is the actual integrand in (47). (The curves in figure 9 are scaled individually for plotting appearances, so that each has the same peak value.) We again observe that the low-order weighted functions are poorly represented by samples taken at $x_n = n\pi$.

For larger arguments x, the "period" P_1 of $J_1(x)$, indicated on figure 8, is approximately 2π; thus, we are getting just 2 samples per period at $\Delta_x = \pi$, which is barely adequate for $J_1(x)$ at large argument values. For the higher-order weighted Bessel functions, the initial peaks (near $x = k+2$) are well represented by samples at $\Delta_x = \pi$. In addition, the period P_2 in figures 8 and 9 is greater than 2π, for larger arguments; thus, we are getting more than 2 samples per period of the higher-order Bessel functions. Of course, eventually, for large enough x, all the $J_k(x)$ have period 2π. (See [6; 9.2.1].)

These sampling considerations indicate that the low-order coefficients $\tilde{a}_q$ will likely be inaccurate, especially when f is near f_o, while the higher-order coefficients will not be badly affected by this particular feature. A numerical investigation of these effects is undertaken in appendix B. In particular, coefficients $\tilde{a}_1$, $\tilde{a}_2$, $\tilde{a}_{10}$ are computed for a variety of values of

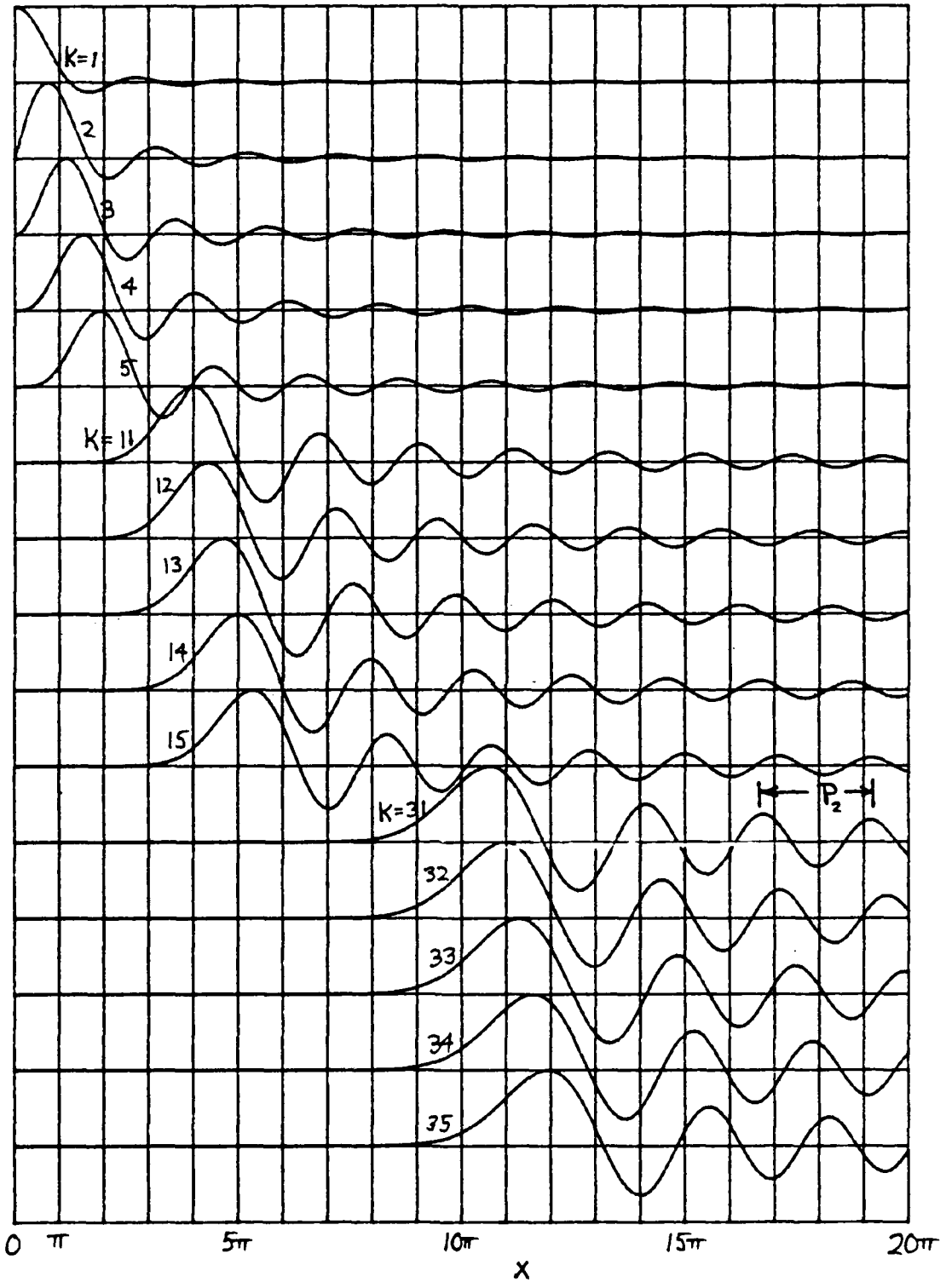

Figure 9. Weighted Functions $J_k(x)/x$

u_o $(\cos\theta_o)$, α $(\pi f/f_o)$, M, and compared with the exact values a_1, a_2, a_{10}. The results quantitatively confirm the above expectations.

The second problem with approximations (58) is that the increment in the samples of spatial correlation C(p) is $\Delta_p = 1$. The discussion surrounding (35) is directly relevant again and should be reviewed. Arrivals near endfire, $\theta_o \sim 0$ or π, will be most severely affected.

A third problem with (58) is that M is not infinite; therefore, the summands may not have decayed sufficiently to terminate the summation at M-1, with negligible error. As seen earlier, for plane-wave arrival (48)-(50), spatial correlation C(p) does not decay at all with p, and since [6; 9.2.1]

$$\frac{J_k(x)}{x} \propto \frac{1}{x^{3/2}} \quad \text{as } x \to +\infty, \tag{60}$$

the integrands of (47) can decay very slowly with p.

Furthermore, if α in (11) is less than π, $J_{2m}(\alpha n)$ and $J_{2m-1}(\alpha n)$ in (58) may not yet have even reached their substantial range of values by the time n reaches M-1. To develop this point, observe from figure 8 that

$$J_k(x) \approx 0 \quad \text{for } |x| < k - 2\pi. \tag{61}$$

Therefore

$$J_{2m}(\alpha n) \approx 0 \quad \text{for } 2m > \alpha n + 2\pi. \tag{62}$$

So, for example, if M = 64 and $f = f_o$, then $\alpha = \pi$, max n = M-1 = 63, and (62) indicates that the Bessel function is essentially zero for 2m > 204. Thus, approximate coefficients $\tilde{a}_q$, determined from (58), will be substantially zero for q > 200; this is the limit that was unknown in [4; under (5b) and bottom of page 1651].

As another example, if M = 64 and $f = f_o/2$, then (62) indicates that the approximate coefficients $\tilde{a}_q$ for q > 105 will be substantially zero; this is verified by [4; figure 3]. Thus, figures 8 and 9, with (62), give a quantitative indication of when the Fourier series method will collapse, in terms of the loss of the higher-order coefficients and the attendant degraded resolution.

RESOLUTION CAPABILITY

The general situation is as follows: approximate coefficient $\tilde{a}_q$ in (58) involves $J_q(\alpha n)$ for n = 1 to M-1. Reference to (61) therefore indicates that if

$$q > \alpha\, n_{max} + 2\pi = \alpha(M-1) + 2\pi \equiv q', \tag{63}$$

then $\tilde{a}_q \simeq 0$. Thus, summation (40) for field $A(\theta)$ will have zero terms for $q > q'$. For the same plane-wave example considered in (48)-(53), this would result in a resolution capability of the order of (appendix A, especially (A-9) and (A-10))

$$\frac{\pi}{q' + \tfrac{1}{2}} \simeq \frac{\pi}{\alpha(M-1)} = \frac{\lambda}{2d(M-1)} = \frac{\lambda}{2L} \tag{64}$$

at broadside, where we used (63), (11), and defined L as the length of the line array. However, the coefficients $\{\tilde{a}_q\}$ deteriorate before q reaches q', typically for $q > q'3/4$. This results in a resolution of the order of

$$\Delta_\theta \simeq \frac{4}{3}\frac{\lambda}{2L} = \frac{2}{3}\frac{\lambda}{L}. \tag{65}$$

This is somewhat sharper than the standard quoted result of λ/L, but not significantly so. Thus, the Fourier series method has slightly better resolution than standard beamforming, which corroborates several of the results in [4].

DISCUSSION

It was demonstrated in (51)-(53), that for the plane-wave arrival of (48)-(50), use of all the exact coefficients $\{a_q\}$ in the Fourier series method restored the field $A(\theta)$ precisely for all θ. However, when we discretize the array and must resort to approximations $\{\tilde{a}_q\}$ in (58), this restoration capability is lost, even if the array is infinitely long; see the tabular results in appendix B for M = 100, 1000, 10000, 100000. This result for the Fourier series method is distinctly different from that for the Fourier integral method, as a review of (21) and figure 3 reveals. In both methods, we are presuming that $f < f_o$, that is, that the array is used at or below its design frequency. Thus, sampling (in space) is more detrimental to the Fourier series method than to the Fourier integral method; this is related to the fact that the latter employs a (single) Fourier transform in (17), whereas the former uses (numerous) Bessel transforms in (47).

The summation on q in (40) for field $A(\theta)$ cannot be carried out to ∞. However, when employed with approximate coefficients $\{\tilde{a}_q\}$, it should be carried out at least to the limit q' given in (63), after which $\{\tilde{a}_q\}$ are essentially zero; this will maximally preserve the resolution capability of the Fourier series method. This procedure was not employed in [4; figures 1,4,6]; thus, some inherent resolution of the Fourier series method was lost in those examples.

GRAPHICAL RESULTS

We shall re-do the examples given in [4], where the Fourier series method was introduced, but now using more coefficients and comparing the results with the Fourier integral method presented here. The first example is that of five plane-waves with arrival angles 54°,57°,60°,63°,66°, as given in [4; figures 1 and 2]. (Angle 90° corresponds to broadside of the line array.) The two arrivals at 57° and 63° each have twice the common power of the other three arrivals. The exact cosine series coefficients $\{a_q\}$ for $0 \le q \le 250$ are plotted in figure 10A, and are listed numerically in table 1 for $0 \le q \le 30$. We have normalized the total power so that the origin value of the spatial correlation is $C(0) = \pi$; then $a_o = \tilde{a}_o = 1$.

For a line array with $M = 64$ elements, employed at its design frequency, $f = f_o$, the approximate coefficients $\{\tilde{a}_q\}$, as determined via (58), are given in figure* 10B and table 1. A comparison of the numerical results in table 1 shows a very large discrepancy between a_1 and $\tilde{a}_1$ and between a_2 and $\tilde{a}_2$. However, this discrepancy decreases to about 5% for $q = 3$ and 4, and is much smaller for $q > 4$. Comparison of the plots in figure 10 reveals that $\tilde{a}_q$ is substantially zero for $q > 205$, in agreement with (62) et seq., and that $\tilde{a}_q$ and a_q are very similar for $2 < q < 175$.

---

*This figure is not in complete agreement with [4; figure 2].

Table 1. Cosine Series Coefficients

q	a_q	$\tilde{a}_q$
0	1.0000	1.0000
1	.9977	.4837
2	-.9906	-.4407
3	-1.9580	-2.0569
4	-.9628	-.9130
5	.9423	.9265
6	1.8349	1.8428
7	.8887	.8868
8	-.8561	-.8535
9	-1.6399	-1.6395
10	-.7806	-.7784
11	.7383	.7390
12	1.3869	1.3895
13	.6463	.6471
14	-.5974	-.5942
15	-1.0938	-1.0933
16	-.4954	-.4916
17	.4431	.4433
18	.7809	.7852
19	.3379	.3376
20	-.2857	-.2810
21	-.4687	-.4697
22	-.1841	-.1793
23	.1353	.1335
24	.1766	.1811
25	.0433	.0406
26	-.0007	.0031
27	.0790	.0754
28	.0769	.0794
29	-.1114	-.1157
30	-.2857	-.2851

For these same parameter values, the reconstructed field distribution, via the Fourier integral method of (32), is depicted in figure 11A, while that for the Fourier series method of (58), (40), and (63), using approximate coefficients $\{\tilde{a}_q\}$, is displayed in figure 11B. This latter figure is an improvement over [4; figure 1] for two reasons: 250 coefficients $\{\tilde{a}_q\}$ were used instead of 140, and the angular sampling increment was

previously insufficient to track the detailed behavior of the field distribution. The two parts of figure 11 are very similar, except for the drift in the Fourier series method near $\theta = \pi$, due mainly to inaccurate low-order coefficients $\tilde{a}_1$ and $\tilde{a}_2$.

Both plots yield some negative values for the reconstructed field distribution, due to sidelobes from the plane-wave components. These can be suppressed at the cost of decreased resolution. See (25)-(31) for the Fourier integral method. As for the Fourier series method, if approximations (58) (to exact results (47)) used a taper, instead of box-car weighting out to $p = M-1$, a similar control of sidelobes is achievable.

If all the parameter values above are kept unchanged, except that the arrival angles are squeezed closer together, namely 56°,58°,60°,62°,64°, we then have the example considered in [4; figures 4 and 5]. The exact and approximate cosine series coefficients are given in figures 12A and 12B, respectively. The field distribution for the Fourier integral method is plotted in figure 13A, while that for the Fourier series method is plotted in figure 13B. All five plane-waves are resolved by both procedures; in fact, the only essential difference is the slight drift in figure 13B near $\theta = \pi$, due to poor values of $\tilde{a}_1$ and $\tilde{a}_2$. Figure 13B is a significant improvement over [4; figure 4], again due to additional coefficients and finer angular sampling in θ.

The third example of the Fourier series method, from [4; figure 6], corresponds to three plane-waves with arrivals closer to endfire, namely 27°,30°,33°. The power level of the

33° arrival is one-half of the common power level of the other two arrivals; all other parameters are unchanged. The exact and approximate coefficients are given in the two parts of figure 14; the approximation appears to deteriorate for q > 100. The field distribution for the Fourier integral method is depicted in figure 15A, while that for the Fourier series method is plotted in figure 15B. The major discrepancy is again the drift in the latter plot near $\theta = \pi$; this is in spite of the seemingly poor results for coefficients $\{\tilde{a}_q\}$ in figure 14B.

The final example considered here is that given in [1; page 15], namely

$$B(u) = \left\{ \begin{array}{ll} 0 & \text{for } -1 < u < 0 \\ 2u & \text{for } 0 < u < 1 \end{array} \right\} . \qquad (66)$$

However, those earlier results were limited to $M \leq 12$ due to ill-conditioning. The spatial correlation follows from (15) as

$$C(p) = \frac{2}{\alpha^2 p^2} \left[\exp(-i\alpha p) \, (1 + i\alpha p) - 1 \right] . \qquad (67)$$

The reconstructed field distribution via the Fourier integral method, for M = 64 elements, is presented in figures 16A and 16B for flat weighting (32), with $f/f_o = 1$ and .5, respectively. The corresponding plots for Hann weighting, (25) and figure 5, are depicted in figure 17. The familiar tradeoff between resolution and sidelobes is quite evident. Perhaps a plot of both results, with and without weighting, would yield important information not available from either plot alone.

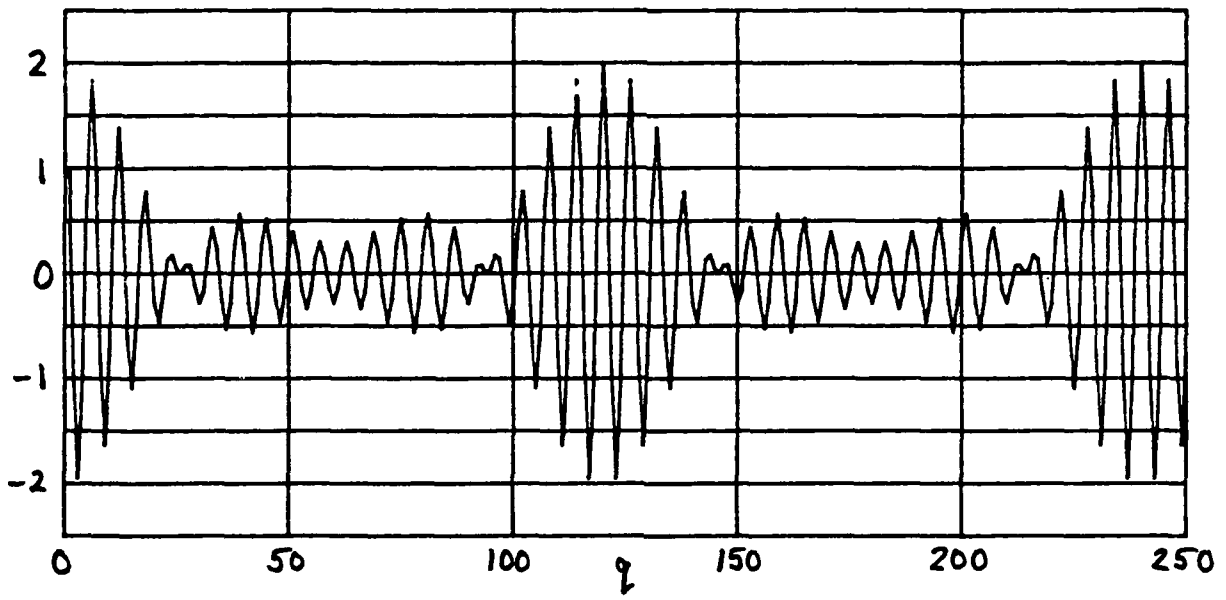

Figure 10A. Coefficients a_q

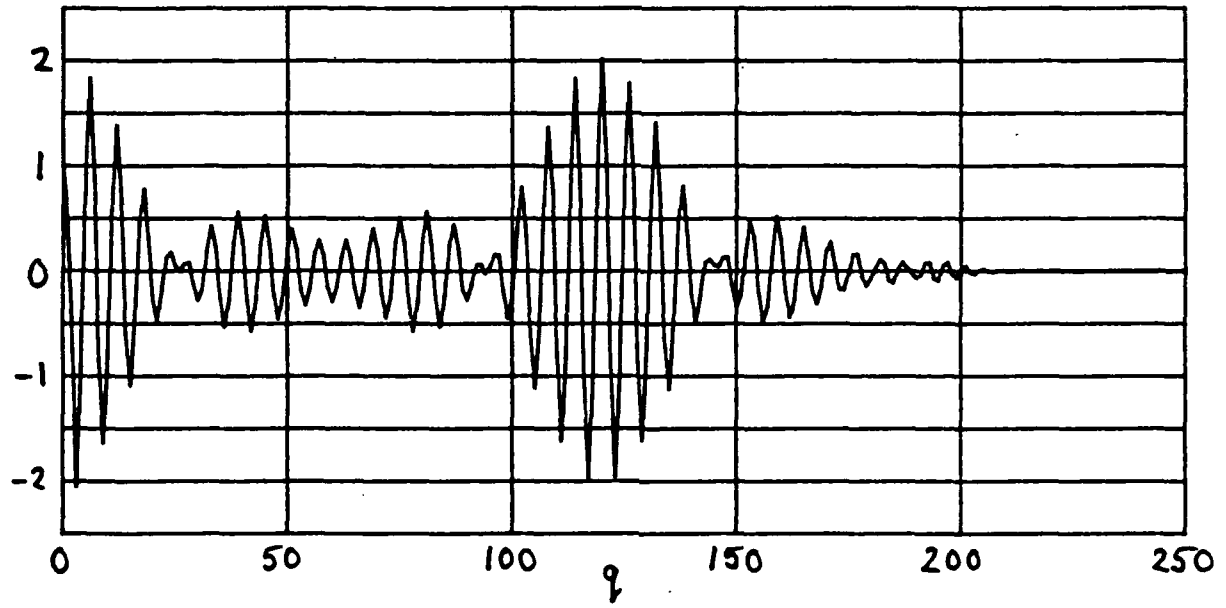

Figure 10B. Coefficients $\tilde{a}_q$

Figure 10. Coefficients for Five Separated Arrivals

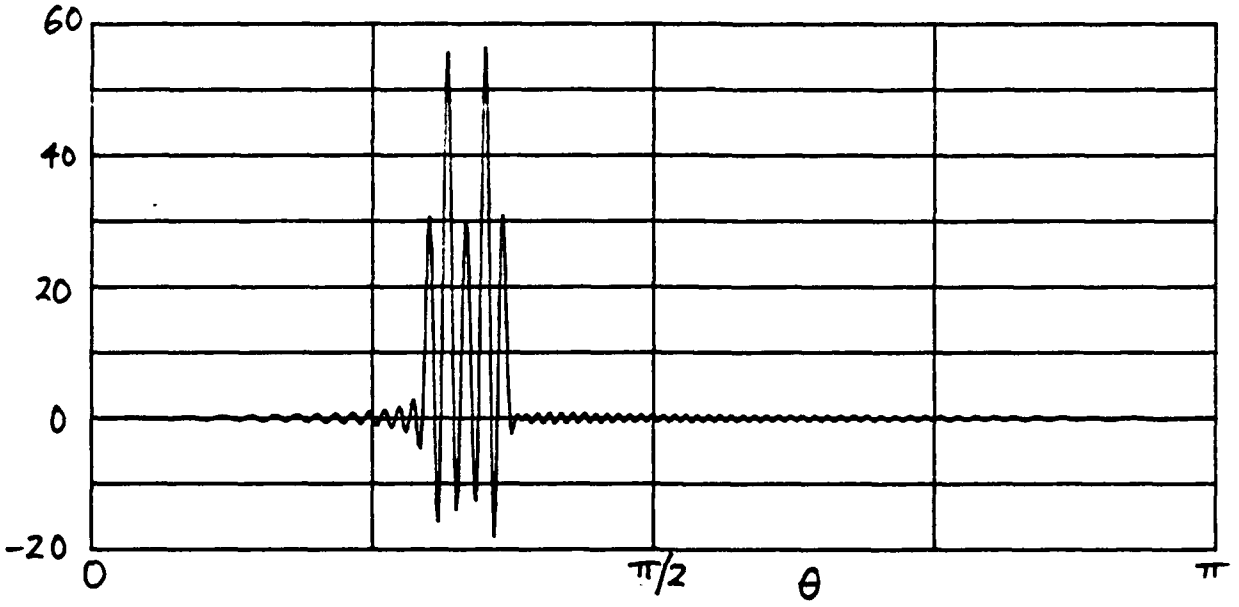

Figure 11A. Fourier Integral Method

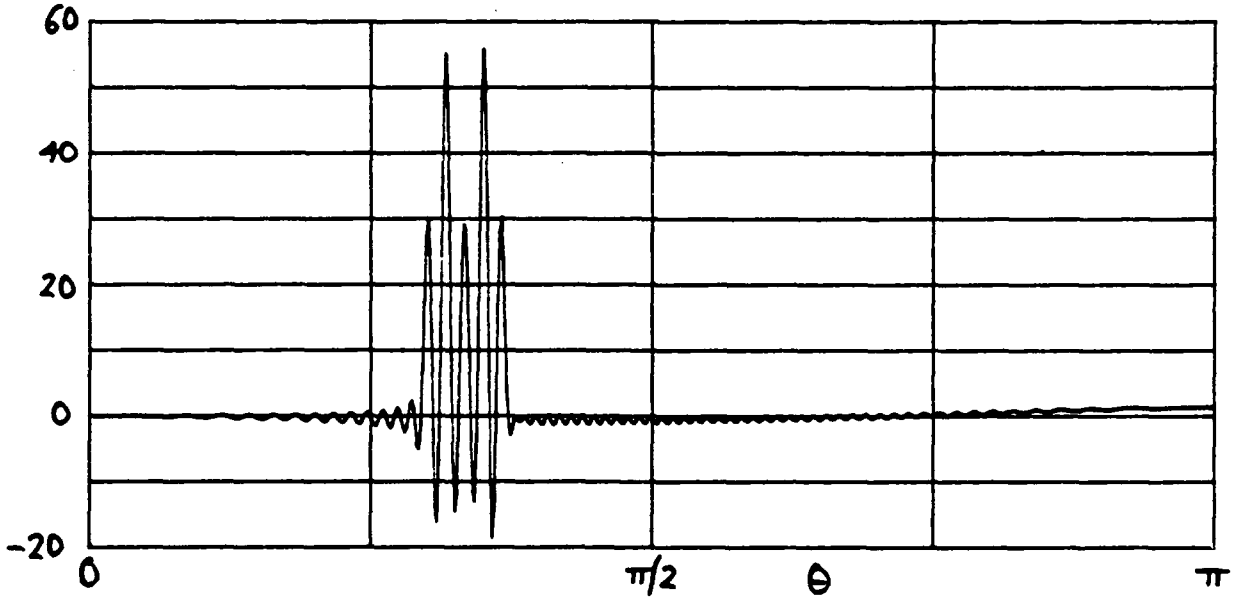

Figure 11B. Fourier Series Method

Figure 11. Directionality for Five Separated Arrivals

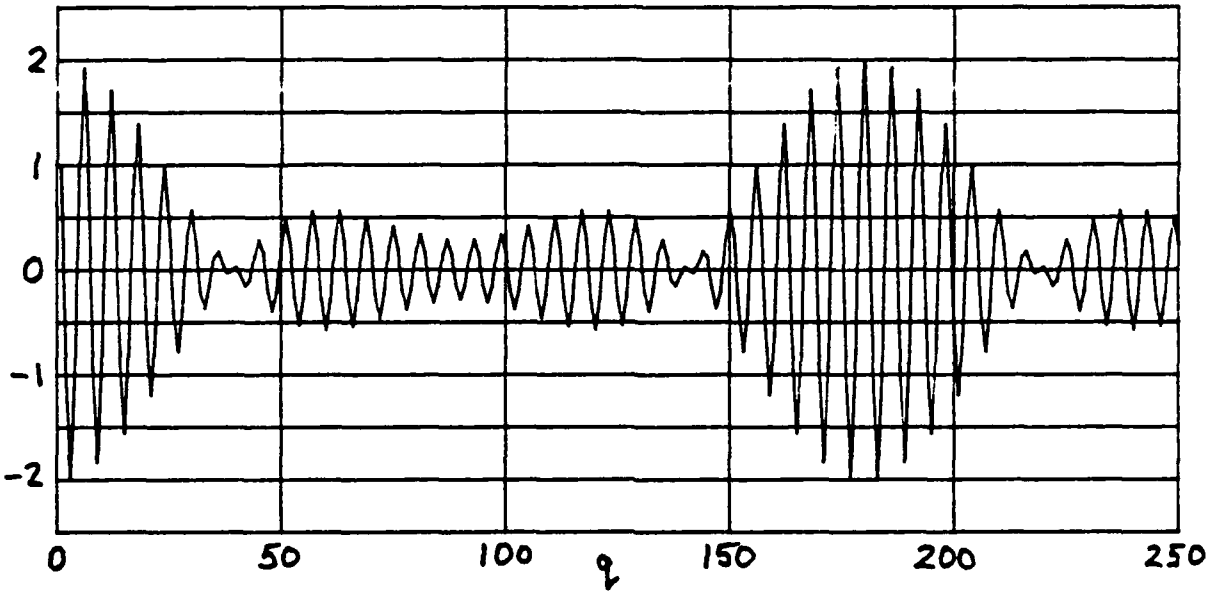

Figure 12A. Coefficients a_q

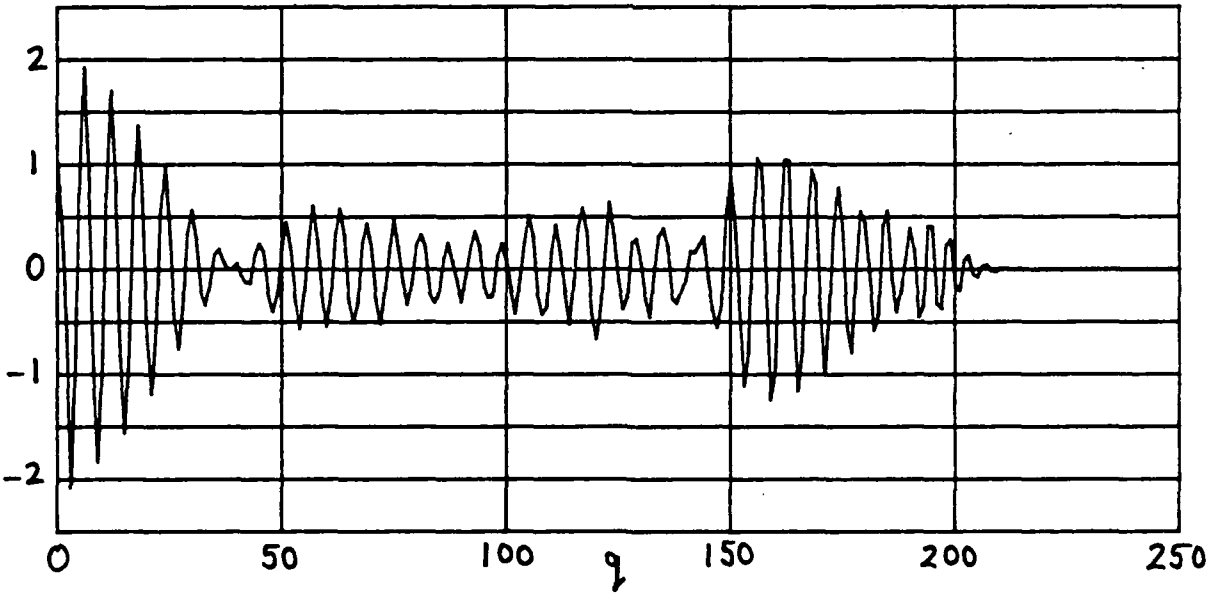

Figure 12B. Coefficients $\tilde{a}_q$

Figure 12. Coefficients for Five Close Arrivals

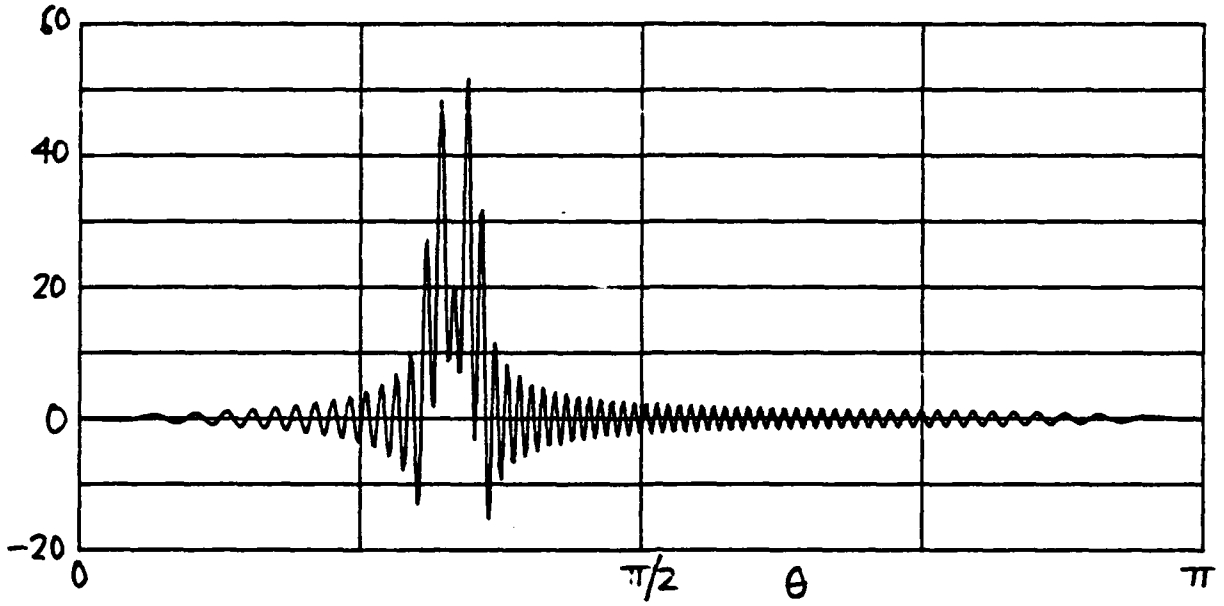

Figure 13A. Fourier Integral Method

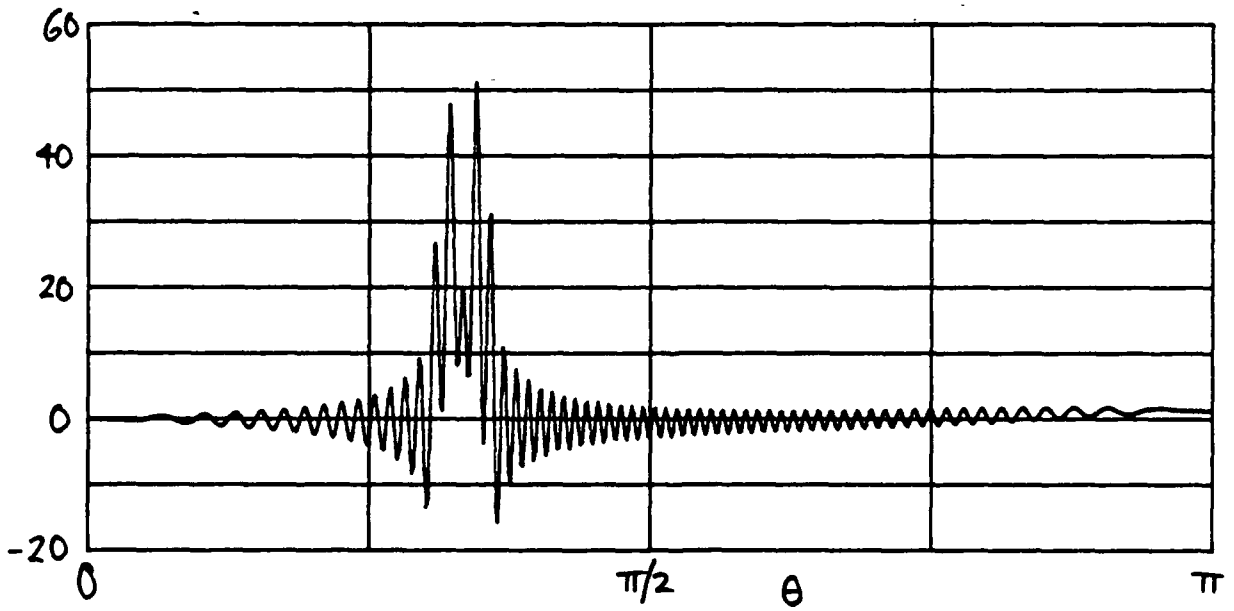

Figure 13B. Fourier Series Method

Figure 13. Directionality for Five Close Arrivals

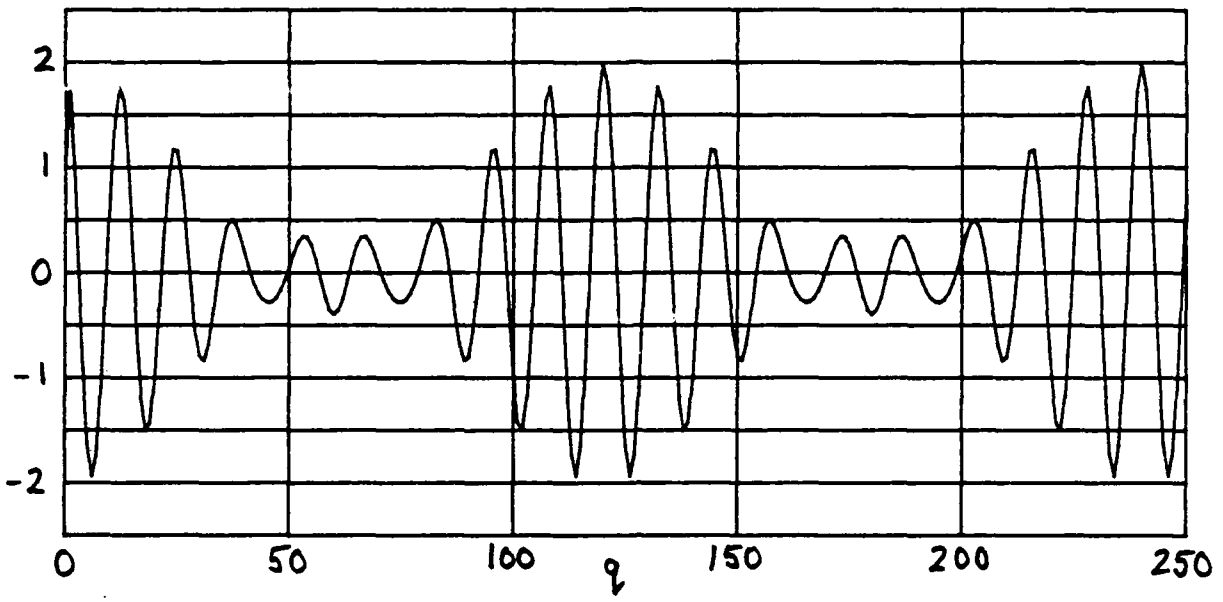

Figure 14A. Coefficients a_q

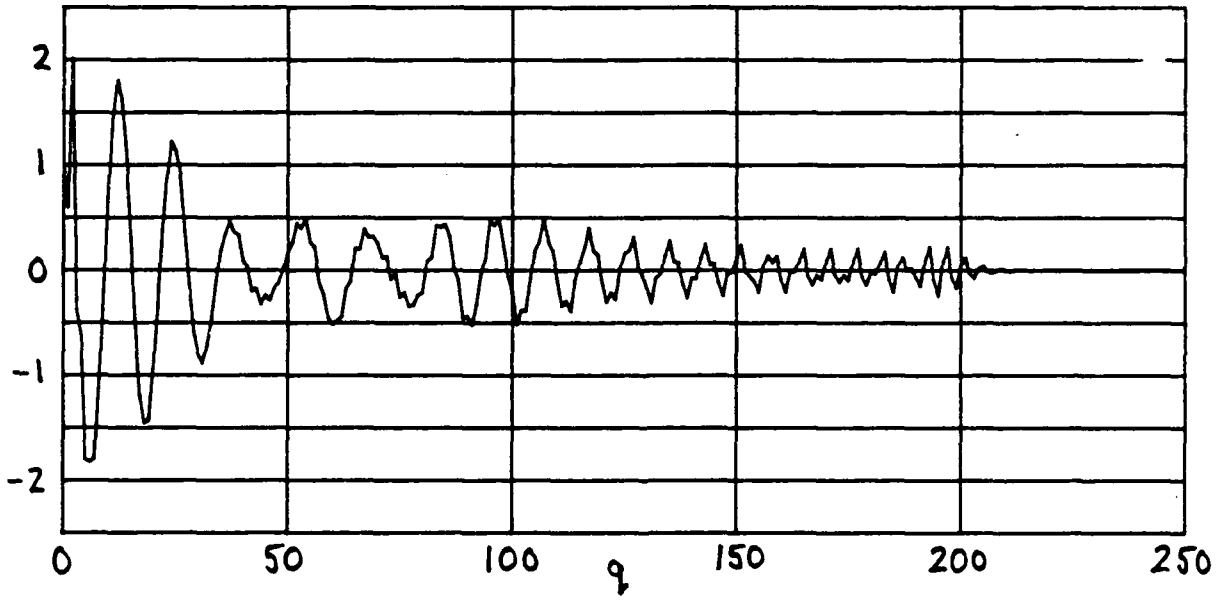

Figure 14B. Coefficients $\tilde{a}_q$

Figure 14. Coefficients for Three Arrivals

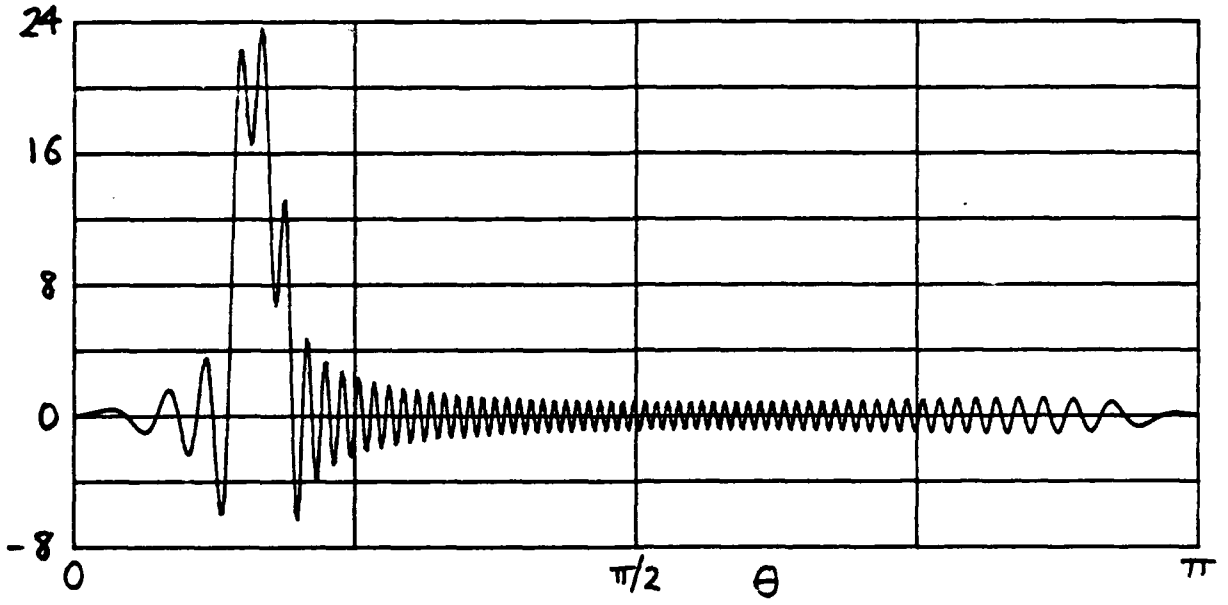

Figure 15A. Fourier Integral Method

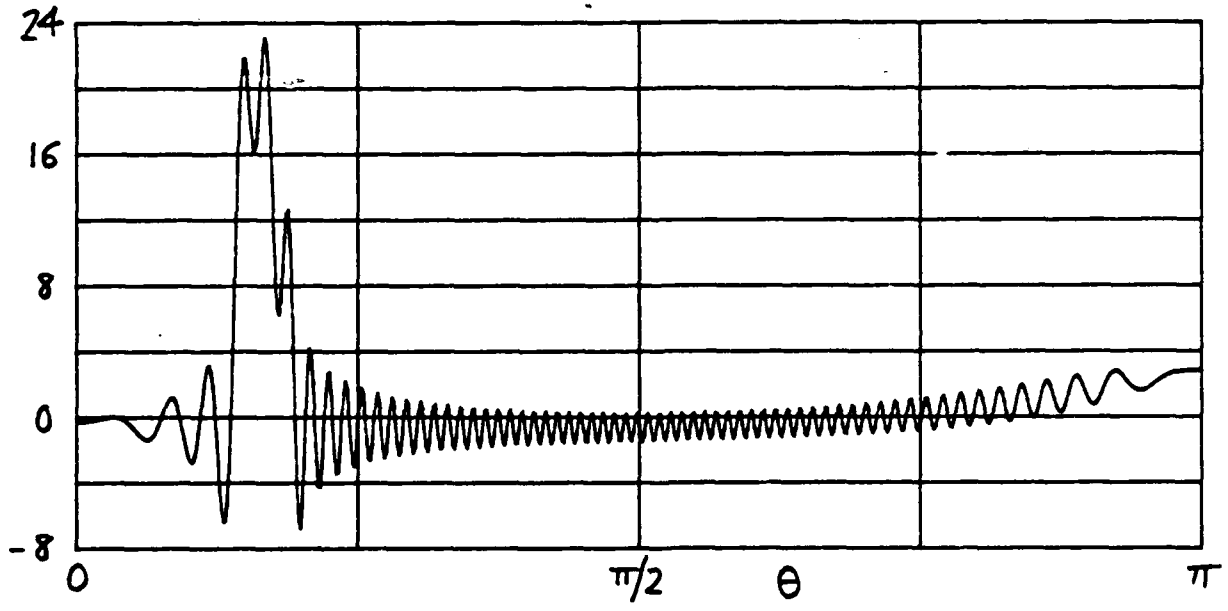

Figure 15B. Fourier Series Method

Figure 15. Directionality for Three Arrivals

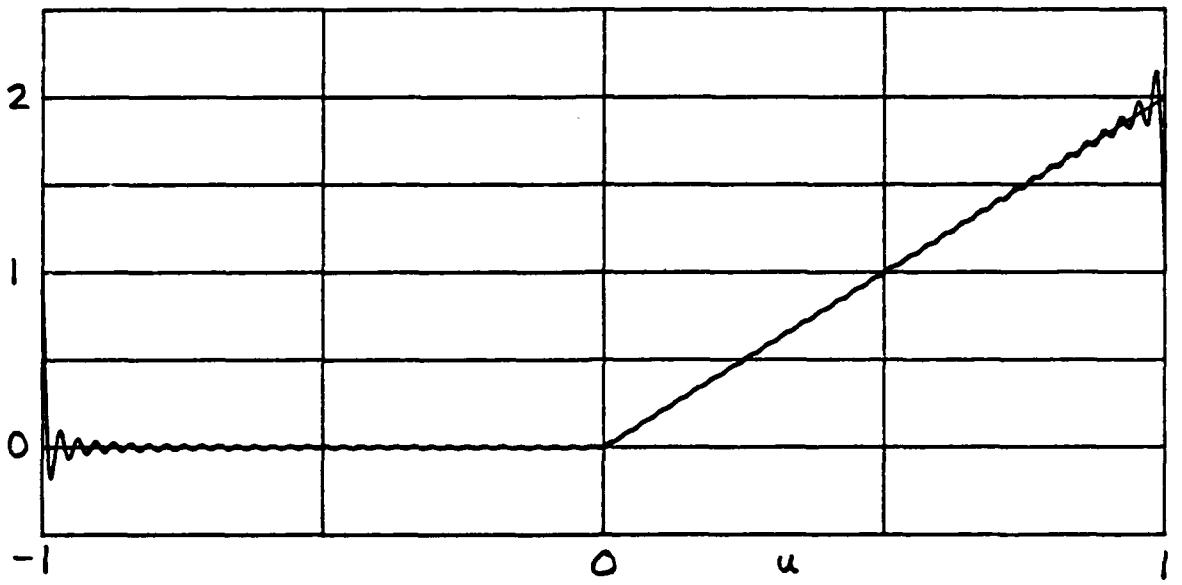

Figure 16A. $f/f_o = 1$

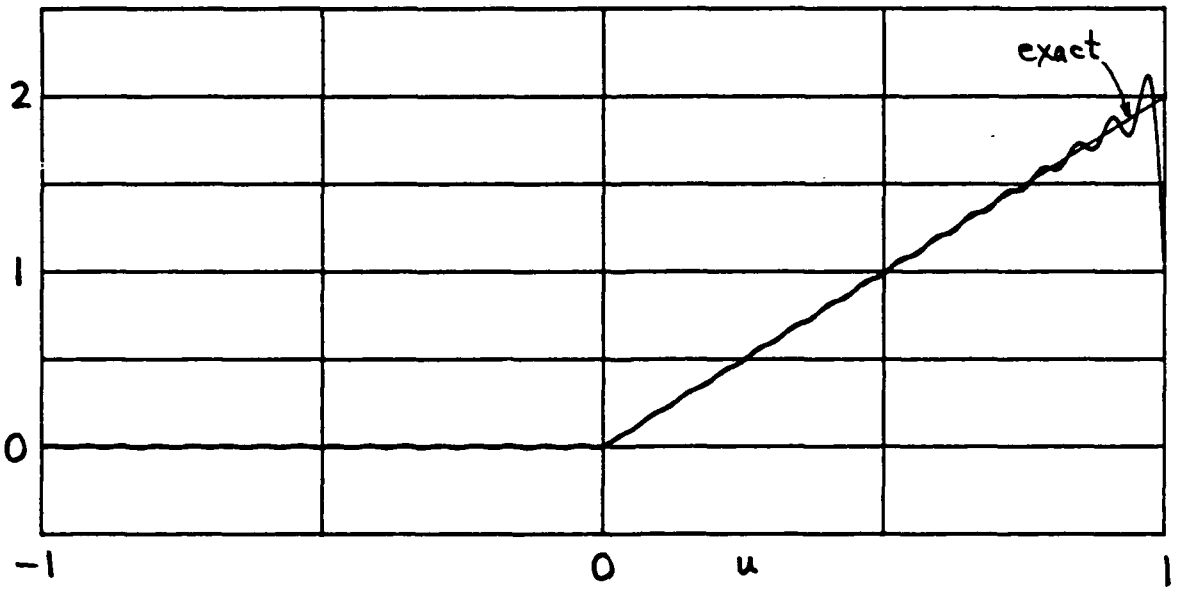

Figure 16B. $f/f_o = .5$

Figure 16. Directionality for Flat Weighting

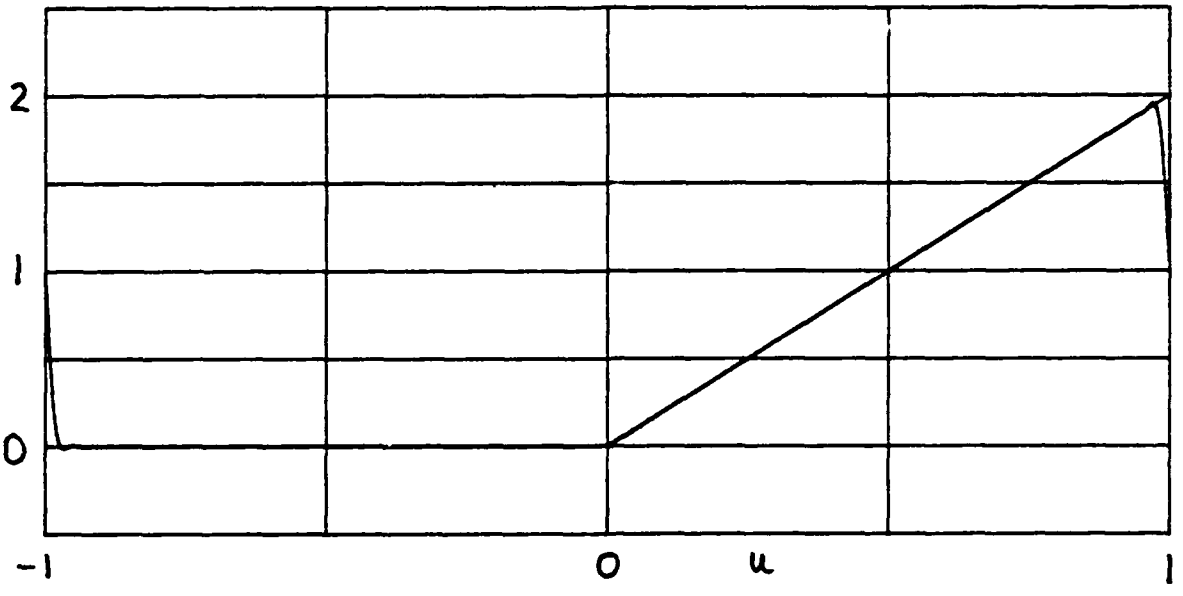

Figure 17A. $f/f_o = 1$

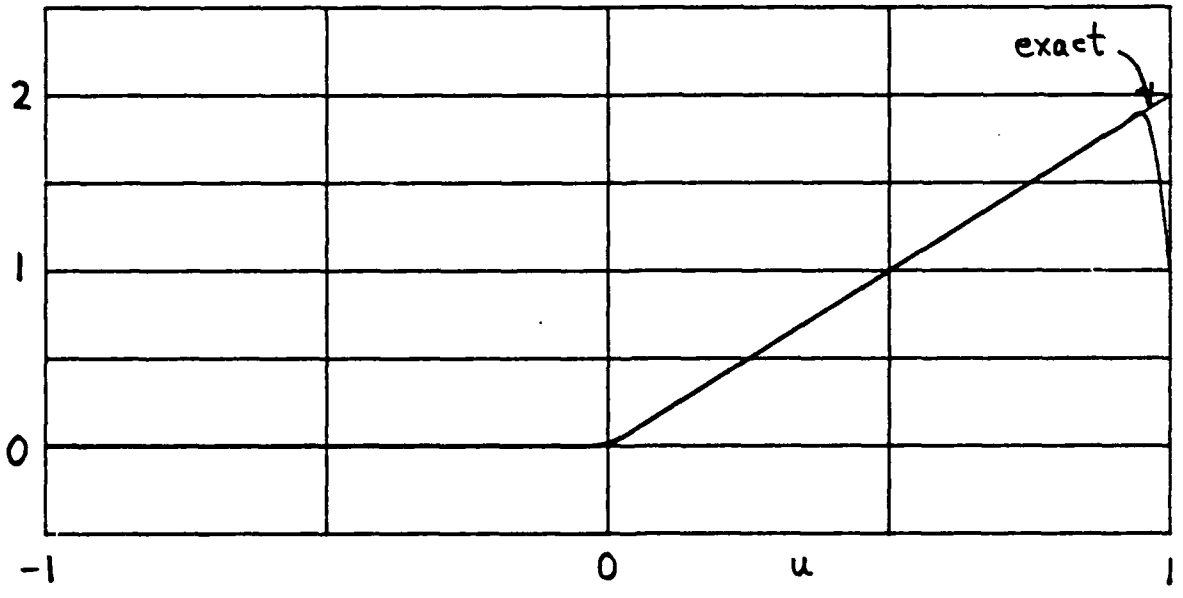

Figure 17B. $f/f_o = .5$

Figure 17. Directionality for Hann Weighting

SUMMARY

The Fourier integral method and the Fourier series method have very similar performance; the major difference is the slow drift in the background level of the noise field directionality for the Fourier series method due to inaccurate low-order cosine series expansion coefficients. There is a rather large difference, however, in terms of the amount of computation, since the Fourier integral method can employ a fast Fourier transform to good advantage, while the Fourier series method requires numerous Bessel function evaluations.

Use of the array somewhat below its design frequency eases the aliasing problems associated with both methods; but there is a tradeoff connected with this approach, namely, a loss of resolution. Similarly, weighting can be used to suppress sidelobes, but again, only at the expense of resolution.

It has been presumed throughout this report that the spatial correlation is known exactly, for all required argument values, without any random error. In practice, the spatial correlation must be estimated from a finite observation time on random processes. This limitation will further degrade the performance of both techniques considered here; which one will suffer most, and by how much, is unknown.

APPENDIX A. EXAMPLE OF FOURIER SERIES METHOD

The single plane-wave arrival was given in (48); it yields spatial correlation (50):

$$C(p) = \exp(-i\alpha p \cos\theta_o); \quad 0 < \theta_o < \pi. \tag{A-1}$$

Substitution in (47) yields coefficients [7; 6.693 2&1]

$$\left.\begin{aligned} a_{2m} &= \frac{2}{\pi}(-1)^m \cos(2m\beta) \\ a_{2m-1} &= \frac{2}{\pi}(-1)^{m-1} \sin[(2m-1)\beta] \end{aligned}\right\} \text{ for } m \geq 1, \tag{A-2}$$

where

$$\beta = \operatorname{asin}(\cos\theta_o) = \frac{\pi}{2} - \theta_o. \tag{A-3}$$

Although spatial correlation C(p) depends on α, coefficients $\{a_q\}$ do not. Also, observe that

$$\cos(2m\beta) = \cos(m\pi - 2m\theta_o) = (-1)^m \cos(2m\theta_o),$$

$$\sin[(2m-1)\beta] = \sin\left[\left(2m-1\right)\left(\frac{\pi}{2} - \theta_o\right)\right] = (-1)^{m-1} \cos[(2m-1)\theta_o], \tag{A-4}$$

giving

$$a_q = \frac{2}{\pi}\cos(q\,\theta_o) \quad \text{for } q \geq 1. \tag{A-5}$$

When these coefficients, along with $a_o = 1/\pi$, are substituted in the right-hand side of (40), we obtain (letting θ be arbitrary)

$$R(\theta) \equiv \frac{1}{\pi} + \frac{2}{\pi} \sum_{q=1}^{+\infty} \cos(q\theta_o)\, \cos(q\theta) =$$

$$= \frac{1}{\pi} + \frac{1}{\pi} \sum_{q=1}^{+\infty} [\cos(q(\theta-\theta_o)) + \cos(q(\theta+\theta_o))]. \qquad \text{(A-6)}$$

But [8; page 28]

$$\frac{1}{2\pi} + \frac{1}{\pi} \sum_{q=1}^{+\infty} \cos(qt) = \frac{1}{2\pi} \sum_{q=-\infty}^{+\infty} \cos(qt) = \sum_{m=-\infty}^{+\infty} \delta(t-m2\pi)\ , \qquad \text{(A-7)}$$

giving

$$R(\theta) = \sum_{m=-\infty}^{+\infty} [\delta(\theta - \theta_o - m2\pi) + \delta(\theta + \theta_o - m2\pi)] \quad \text{for all } \theta. \qquad \text{(A-8)}$$

This function is discussed in (52) et seq.

For future reference, if the sum in (A-7) were terminated at q′, we have

$$\frac{1}{2\pi} + \frac{1}{\pi} \sum_{q=1}^{q'} \cos(qt) = \frac{1}{2\pi} \frac{\sin[(2q'+1)t/2]}{\sin(t/2)}\ . \qquad \text{(A-9)}$$

The first zero crossing of this function is at

$$t_o = \frac{\pi}{q'+\frac{1}{2}}\ . \qquad \text{(A-10)}$$

This is approximately the resolution of waveform (A-9).

APPENDIX B. NUMERICAL INVESTIGATION OF (58)

For the single plane-wave arrival given in (48)-(50), the spatial correlation is

$$C(p) = \exp(-i\alpha p u_o) , \quad \alpha = \pi f/f_o , \quad |u_o| < 1. \qquad (B-1)$$

Substitution in (58) gives approximate coefficients

$$\frac{\pi}{2}\,\tilde{a}_1 = \sum_{n=1}^{M-1} \frac{J_1(\alpha n)}{n} \sin(\alpha n u_o) ,$$

$$\frac{\pi}{2}\,\tilde{a}_2 = -2\sum_{n=1}^{M-1} \frac{J_2(\alpha n)}{n} \cos(\alpha n u_o) ,$$

$$\frac{\pi}{2}\,\tilde{a}_{10} = -10\sum_{n=1}^{M-1} \frac{J_{10}(\alpha n)}{n} \cos(\alpha n u_o) . \qquad (B-2)$$

The exact coefficients are given by (51) as

$$\frac{\pi}{2}\,a_q = \cos(q\theta_o) = \cos(q\ \mathrm{acos}(u_o)) \quad \text{for } q \geq 1 , \qquad (B-3)$$

and are independent of α.

Numerical values of approximations (B-2) are given in tables B-1, B-2, B-3, respectively, for several values of u_o, α, and for $M = 100, 1000, 10000, 100000$. The exact values, from (B-3), are listed in the right-most column for comparison purposes.

Several observations can be made from these tables. Except for $u_o = 1$, the sums in (B-2) for $M = 100$ are not too different from what they would have been for $M = \infty$. Part of this is due to the fact that $M = 100$ is considerably larger than the biggest coefficient order, 10, that we considered here.

The values of the approximate coefficients $\tilde{a}_1$ and $\tilde{a}_2$ are poor for $\alpha = \pi$, that is, for frequency f equal to design frequency f_o, even for a large number of elements M, independent of arrival angle u_o. However, if α is decreased, so that f is well below the design frequency f_o, $d < \lambda/2$, then $\tilde{a}_1$ and $\tilde{a}_2$ are rather close to a_1 and a_2, respectively. However, the loss in resolution is unlikely to be tolerable in this case.

By contrast, the values of $\tilde{a}_{10}$ in table B-3 are good approximations to a_{10}, with two exceptions:

$$u_o = 1, \quad \alpha = \pi, \quad \text{all } M \ ;$$

$$u_o = 1, \quad \text{all } \alpha, \quad M = 100 \ . \qquad \text{(B-4)}$$

That is, endfire arrivals will cause the most problems, as is expected physically.

Table B-1. Values of $\frac{\pi}{2}\,\tilde{a}_1$

u_o	α	$\frac{\pi}{2}\,\tilde{a}_1$ for: M=100	M=1000	M=10000	M=100000	$\frac{\pi}{2}\,a_1$
0	all	0	0	0	0	0
.25	π	.129232	.129164	.129166	.129166	.25
.25	.75π	.187050	.187166	.187169	.187169	.25
.25	.5π	.223371	.223390	.223387	.223387	.25
.25	.25π	.244032	.243504	.243520	.243520	.25
.5	π	.243202	.243356	.243361	.243361	.5
.5	.75π	.371340	.371278	.371273	.371273	.5
.5	.5π	.446531	.446295	.446302	.446302	.5
.5	.25π	.487704	.487032	.487014	.487014	.5
.75	π	.312112	.311716	.311728	.311728	.75
.75	.75π	.548651	.548352	.548355	.548355	.75
.75	.5π	.668571	.668247	.668229	.668230	.75
.75	.25π	.730345	.730503	.730458	.730456	.75
1	π	0	0	0	0	1
1	.75π	.675038	.700277	.708228	.710741	1
1	.5π	.843507	.874322	.884057	.887135	1
1	.25π	.910216	.953689	.967453	.971806	1

Table B-2. Values of $\frac{\pi}{2}\,\tilde{a}_2$

u_o	α	$\frac{\pi}{2}\,\tilde{a}_2$ for: M=100	M=1000	M=10000	M=100000	$\frac{\pi}{2}\,a_2$
0	π	-.774782	-.774469	-.774460	-.774459	-1
0	.75π	-.877975	-.878516	-.878500	-.878500	-1
0	.5π	-.948405	-.947527	-.947499	-.947498	-1
0	.25π	-.984898	-.987151	-.987084	-.987082	-1
.25	π	-.638731	-.639064	-.639054	-.639054	-.875
.25	.75π	-.751196	-.750903	-.750906	-.750907	-.875
.25	.5π	-.822242	-.822027	-.822058	-.822057	-.875
.25	.25π	-.860117	-.862071	-.862055	-.862057	-.875
.5	π	-.226752	-.226437	-.226428	-.226427	-.5
.5	.75π	-.367826	-.367496	-.367515	-.367515	-.5
.5	.5π	-.444596	-.445729	-.445695	-.445694	-.5
.5	.25π	-.485886	-.486894	-.486983	-.486980	-.5
.75	π	.497761	.497414	.497424	.497425	.125
.75	.75π	.275027	.273883	.273906	.273905	.125
.75	.5π	.182765	.181761	.181708	.181709	.125
.75	.25π	.136903	.138239	.138154	.138149	.125
1	π	1.992866	2.080480	2.108031	2.116738	1
1	.75π	1.105007	1.155646	1.171553	1.176580	1
1	.5π	.969535	1.031886	1.051378	1.057535	1
1	.25π	.884033	.973009	1.000600	1.009308	1

Table B-3. Values of $\frac{\pi}{2}\,\tilde{a}_{10}$

u_o	α	$\frac{\pi}{2}\,\tilde{a}_{10}$ for: M=100	M=1000	M=10000	M=100000	$\frac{\pi}{2}\,a_{10}$
0	π	-1.001835	-1.000047	-.999998	-.999996	-1
0	.75π	-.997211	-1.000083	-1.000002	-1.000000	-1
0	.5π	-1.004328	-1.000142	-1.000004	-1.000000	-1
0	.25π	-.993657	-1.000337	-1.000013	-1.000003	-1
.25	π	.818745	.816853	.816903	.816904	.816895
.25	.75π	.815431	.816916	.816897	.816895	.816895
.25	.5π	.815723	.817043	.816890	.816894	.816895
.25	.25π	.823767	.816816	.816904	.816892	.816895
.5	π	-.501787	-.499985	-.499935	-.499934	-.5
.5	.75π	-.501841	-.499903	-.500002	-.499999	-.5
.5	.5π	-.495030	-.500171	-.500005	-.500000	-.5
.5	.25π	-.492036	-.499587	-.500016	-.500003	-.5
.75	π	.589326	.587351	.587401	.587402	.586426
.75	.75π	.592357	.586315	.586433	.586429	.586426
.75	.5π	.593192	.586680	.586418	.586426	.586426
.75	.25π	.593387	.586898	.586445	.586423	.586426
1	π	1.329489	1.797572	1.936303	1.979867	1
1	.75π	.606719	.882941	.963235	.988393	1
1	.5π	.504084	.856082	.954934	.985763	1
1	.25π	.252087	.794347	.936197	.979862	1

REFERENCES

1. A. H. Nuttall, **Estimation of Noise Directionality Spectrum**, NUSC Technical Memorandum TC-211-71, Naval Underwater Systems Center, New London, CT, 29 October 1971; also NUSC Technical Report 4345, 1 September 1972.

2. A. H. Nuttall, **Estimation of Noise Directionality Spectrum; Extensions and Generalizations**, NUSC Technical Memorandum TC-6-73, Naval Underwater Systems Center, New London, CT, 7 May 1973.

3. N. Yen, **Ambient Sea Noise Directionality: Measurement and Processing**, NUSC Technical Report 5545, Naval Underwater Systems Center, New London, CT, 28 February 1977.

4. J. H. Wilson, "Signal Detection and Localization Using the Fourier Series Method (FSM) and Cross-Sensor Data," **Journal of the Acoustical Society of America**, volume 73, number 5, pages 1648-1656, May 1983.

5. F. B. Hildebrand, **Methods of Applied Mathematics**, Prentice-Hall, Inc., New York, NY, 1954.

6. **Handbook of Mathematical Functions**, U. S. Department of Commerce, National Bureau of Standards, Applied Mathematics Series No. 55, U. S. Government Printing Office, Washington, DC, June 1964.

7. I. S. Gradshteyn and I. M. Ryzhik, **Table of Integrals, Series and Products**, Academic Press, New York, NY, 1980.

8. P. M. Woodward, **Probability and Information Theory, with Applications to Radar**, Pergamon Press, New York, NY, 1957.

REFERENCES (cont'd)

9. A. H. Nuttall, **Determination of Noise Field Directionality Directly from Spatial Correlation for Linear, Planar, and Volumetric Arrays**, NUSC Technical Report 8631, Naval Underwater Systems Center, New London, CT, 6 October 1989.

A. H. Nuttall

INITIAL DISTRIBUTION LIST

Addressee	No. of Copies
ADMIRALTY RESEARCH ESTABLISHMENT, London, England (Dr. L. Lloyd)	1
ADMIRALTY UNDERWATER WEAPONS ESTABLISHMENT, Dorset, England	1
APPLIED PHYSICS LAB, JOHN HOPKINS (John C. Stapleton)	1
APPLIED PHYSICS LAB, U. WASHINGTON (C. Eggan)	1
APPLIED RESEARCH LAB, PENN STATE,(Frank W. Symons)	1
APPLIED RESEARCH LAB, U. TEXAS (Dr. M. Frazer)	1
APPLIED SEISMIC GROUP, Cambridge, MA (Richard Lacoss)	1
A & T, Stonington, Ct (H. Jarvis)	1
ASTRON RESEARCH & ENGINEERING, Santa Monica, CA (Dr. Allen Piersol)	1
BBN, Arlington, Va. (Dr. H. Cox)	1
BBN, Cambridge, MA (H. Gish)	1
BBN, New London, Ct. (Dr. P. Cable)	1
BELL COMMUNICATIONS RESEARCH, Morristown, NJ (J. Kaiser and D. Sunday (Library)	2
BENDAT, Julius Dr., Los Angeles, CA	1
BLEINSTEIN, Norman Dr., Denver, CO	1
BROWN UNIV, Providence, RI (Documents Library)	1
CANBERRA COLLEGE OF ADV. EDUC, BELCONNEN, A.C.T. Australia (P. Morgan)	1
COAST GUARD ACADEMY, New London, CT (Prof. J. Wolcin)	1
COAST GUARD R & D, Groton, CT (Library)	1
COGENT SYSTEMS, INC, (J. Costas)	1
COHEN, Leon Dr., Bronx, NY	1
CONCORDIA UNIVERSITY H-915-3, Montreal, Quebec Canada (Prof. Jeffrey Krolik)	1
CNO (NOP-098)	1
CNR-OCNR-00, 10, 12, 13, 20	5
DALHOUSIE UNIV., Halifax, Nova Scotia, Canada (Dr. B. Ruddick)	1
DAVID W. TAYLOR RESEARCH CNTR, Annapolis, MD (P. Prendergast, Code 2744)	1
DARPA, Arlington, VA (A. Ellinthorpe)	1
DEFENCE RESEARCH CENTER, Adeliade, Australia (Library	1
DEFENCE RESEARCH ESTAB. ATLANTIC, Dartmouth, Nova Scotia (Library)	1
DEFENCE RESEARCH ESTAB. PACIFIC, Victoria, Canada (Dr. D. Thomson)	1
DEFENCE SCIENTIFIC ESTABLISHMENT, MINISTRY OF DEFENCE, Auckland, New Zealand (Dr. L. Hall)	1
DEFENSE SYSTEMS, INC, Mc Lean, VA (Dr. G. Sebestyen)	1
DIA	1
DIAGNOSTIC/RETRIEVAL SYSTEMS, INC, Tustin, CA. (J. Williams)	1
DTIC	1
DTRC	1
DREXEL UNIV, (Prof. S. Kesler)	1
EDO CORP, College Point, NY (M. Blanchard)	1

INITIAL DISTRIBUTION LIST (Cont'd.)

Addressee	No. of Copies
EG&G, Manassas, VA (D. Frohman)	1
GENERAL ELECTRIC CO, Moorestown, NJ (Dr. Mark Allen 108-102)	1
GENERAL ELECTRIC CO., Philadelphia, PA (T. J. McFall)	1
GENLRAL ELECTRIC CO, Pittsfield, MA (R. W. Race)	1
GENERAL ELECTRIC CO, Syracuse, NY (J. L. Rogers, Dr. A. M. Vural and D. Winfield)	3
HAHN, Wm, Wash, DC	1
HARRIS SCIENTIFIC SERVICES, Dobbs Ferry, NY (B. Harris)	1
HARVARD UNIVERSITY, Gordon McKay Library	1
HONEYWELL ENGR SERV CNTR, Poulsbro, WA (C. Schmid)	1
HUGHES AIRCRAFT, Fullerton, CA (S. Autrey)	1
HUGHES AIRCRAFT, Buena Park, CA (T. Posch)	1
IBM, Manassas, VA (G. Demuth)	1
INDIAN INSTITUTE OF TECHNOLOGY, Madras, India (Dr. K. M. M. Prabhu)	1
INTERSTATE ELECTRONICS CORP, Anaheim, CA (R. Nielsen, 8011)	1
JOHNS HOPKINS UNIV, Laurel, MD (J. C. Stapleton)	1
KILDARE CORP, New London, CT (Dr. R. Mellen)	1
LINCOM CORP., Northboro, MA (Dr. T. Schonhoff)	1
MAGNAVOX ELEC SYSTEMS CO, Ft. Wayne, IN (R. Kenefic)	1
MALTZ, FRED, Sunnyvale, CA	1
MARINE BIOLOGICAL LAB, Woods Hole, MA	1
MARINE PHYSICAL LABORATORY SCRIPPS	1
MASS. INSTITUTE OF TECHNOLOGY (Prof. A. Baggaroer, Barker Engineering Library)	2
MBS SYSTEMS, Norwalk, CT (A. Winder)	1
MIDDLETON, DAVID, NY, NY	1
NADC (5041, M. Mele)	1
NAIR-03	1
NASH, Harold E., Quaker Hill, CT	1
NATIONAL RADIO ASTRONOMY OBSERVATORY, Charlottesville, VA (F. Schwab)	1
NATIONAL SECURITY AGENCY, FT. Meade, MD (Dr. James R. Maar, R51)	1
NATO SACLANT ASW RESEARCH CENTRE, APO NY, NY (Library, R. E. Sullivan and G. Tacconi)	3
NAVAL OCEAN SYSTEMS CENTER, San Diego, CA (J. M. Alsup, Code 635	1
NCSC	1
NEPRF	1
NORDA	1
NRS, Washington, DC (Dr. Philip B. Abraham, Code 5131)	1
NRL UND SOUND REF DET, Orlando, FL	1
NAVAL INTELLIGENCE COMMAND	1
NAVAL INTELLIGENCE SUPPORT CENTER	1
NAVAL OCEAN SYSTEMS CENTER, San Diego, CA (James M. Alsup, Code 635)	1
NAVAL OCEANOGRAPHY OFFICE	1
NAVAL SYSTEMS DIV., SIMRAD SUBSEA A/S, Norway (E. B. Lunde)	1

INITIAL DISTRIBUTION LIST (Cont'd.)

Addressee	No. of Copies
NICHOLS RESEARCH CORP., Wakefield, MA (T. Marzetta)	1
NORDA (Dr. B. Adams)	1
NORDA (Code 345) N STL Station, MS (R. Wagstaff)	1
NORTHEASTERN UNIV. Boston, MA (Prof. C. L. Nikias)	1
NORWEGIAN DEFENCE RESEARCH EST, Norway (Dr J. Glattetre)	1
NOSC, (James M. Alsup, Code 635, C. Sturdevant; 73, J. Lockwood, F. Harris, 743, R. Smith; 62, R. Thuleen)	6
NPRDC	1
NPS, Monterey, CA (C. W. Therrien, Code 62 Ti)	2
NRL, Washington, DC (Dr. J. Buccaro, Dr. E. Franchi, Dr. P. Abraham, Code 5132, A. A. Gerlach, W. Gabriel (Code 5370), and N. Yen (Code 5130)	6
NRL, Arlington, VA (N. L. Gerr, Code 1111)	1
NSWC	1
NSWC DET Ft. Lauderdale	1
NSWC WHITE OAK LAB	1
NUSC DET TUDOR HILL	1
NUSC DET WEST PALM BEACH (Dr. R. Kennedy Code 3802)	1
NWC	1
ORI CO, INC, New London, CT (G. Assard)	1
ORINCON CORP., Columbia, MD (S. Larry Marple)	1
PAPOUTSANIS, P. D., Athens, Greece	1
PENN STATE UNIV., State College, PA (F. Symons)	1
PIERSOLL ENGR CO, Woodland Hills, CA (Dr. Allen G. Piersol)	1
POHLER, R., Austin, TX	1
POLETTI, Mark A., Acoustics Research Centre, School of Architecture, Univ. of Auckland, Auckland, New Zealand	1
PROMETHEUS, INC, Sharon, MA (Dr. J. Byrnes)	1
PROMETHEUS INC, Newport, RI (Michael J. Barrett)	1
PRICE, Robert Dr. Lexington, MA	1
PURDUE UNIV, West Lafayette, IN (N. Srinivasa)	1
RAISBECK, Dr. Gordon, Portland, ME	1
RAN RESEARCH LAB, Darlinghurst, Australia	1
RAYTHEON CO, Portsmouth, RI (J. Bartram, R. Connor) and S. S. Reese)	3
RICHTER, W., Annandale, VA.	1
ROCKWELL INTERNATIONAL CORP, Anaheim, CA (L. Einstein and Dr. D. Elliott)	2
ROYAL MILITARY COLLEGE OF CANADA, (Prof. Y. Chan)	1
RUTGERS UNIV., Piscataway, NJ (Prof. S. Orfanidis)	1
RCA CORP, Moorestown, NJ (H. Upkowitz)	1
SACLANT UNDERSEA RESEARCH CENTRE, APO NY NY (Dr. John Ianniello, Dr. S. Stergiopolous and Giorgio Tacconi, Library	4
SAIC, Falls Church, VA (Dr. P. Mikhalevsky)	1
SAIC, New London, CT (Dr. F. Dinapoli)	1
SANDIA NATIONAL LABORATORY (J. Claasen)	1
SCHULKIN, Dr. Morris, Potomac, MD	1
SEA-00, 63, 63X	3
SIMON FRASER UNIV, British Columbia, Canada (Dr. Edgar Velez)	1

INITIAL DISTRIBUTION LIST (Cont'd.)

Addressee	No. of Copies
SONAR SURVEILLANCE GROUP, Darlinghurst, Australia	1
SOUTHEASTERN MASS. UNIV (Prof. C. H. Chen)	1
SPAWARS-00, 04, 005, PD-80 and PMW-181	5
SPERRY CORP, Great Neck, NY	1
STATE UNIV. OF NY AT STONY BROOK (Prof. M. Barkat)	1
TEL-AVIV UNIV, Tel-Aviv, Israel (Prof. E. Winstein)	1
TOYON RESEARCH CORP, Goleta, CA (M. Van Blaricum)	1
TRACOR, INC, Austin, TX (Dr. T Leih and J. Wilkinson)	2
TRW FEDERAL SYSTEMS GROUP, Fairfax, VA (R. Prager)	1
UNITED ENGINEERING CENTER, Engr. Societies Library, NY, NY	1
UNIV. OF AUCKLAND, New Zealand (Dr. Murray D. Johns)	1
UNIV. OF ALBERTA, Edmonton, Alberta, CANADA (K. Yeung)	1
UNIV OF CA, San Diego, CA (Prof. C. Helstrom)	1
UNIV OF COLORADO, Boulder, CO (Prof. L. Scharf)	1
UNIV. OF CT, Storrs, CT. (Library and Prof. C. Knapp)	2
UNIV OF FLA, Gainesville, FL (D. Childers)	1
UNIV OF ILLINOIS, Urbana, IL 61801 (Dr. Douglas L. Jones)	1
UNIV OF MICHIGAN, Ann Arbor, MI (William J. Williams)	1
UNIV. OF MINN, Minneapolis, Mn (Prof. M. Kaveh)	1
UNIV. OF NEWCASTLE, Newcastle, NSW, Canada (Prof. A. Cantoni)	1
UNIV. OF QUEENSLAND, St. Lucia, Queensland 4067, Australia (Dr. Boualem Boashash)	1
UNIV. OF RI, Kingston, RI (Prof. G. F. Boudreaux-Bartels, Library, Prof. S. Kay, and Prof. D. Tufts)	4
UNIV. OF ROCHESTER, Rochester, NY (Prof. E. Titlebaum)	1
UNIV. OF SOUTHERN CA., LA. (Prof. William C. Lindsey, Dr. Andreas Polydoros, PHE 414)	2
UNIV. OF STRATHCLYDE, ROYAL COLLEGE, Glasgow, Scotland (Prof. T. Durrani)	1
UNIV. OF TECHNOLOGY, Loughborough, Leicestershire, England (Prof. J. Griffiths)	1
UNIV. OF WASHINGTON, Seattle (Prof. D. Lytle)	1
URICK, ROBERT, Silver Springs, MD	1
US AIR FORCE, Maxwell AF Base, AL (Library)	1
VAN ASSELT, Henrik, USEA S.P.A., La Spezia, Italy	1
VILLANOVA UNIV, Villanova, PA (Prof. Moeness G. Amin)	1
WEAPONS SYSTEMS RESEARCH LAB, Adelaide, Australia	2
WERBNER, A., Medford, MA	1
WESTINGHOUSE ELEC. CORP, OCEANIC DIV, Annapolis, MD (Dr. H. Newman and Dr. H. L. Price)	2
WESTINGHOUSE ELEC. CORP, Waltham, MA (D. Bennett)	1
WILSON JAMES H., San Clemente, CA	1
WOODS HOLE OCEANOGRAPHIC INSTITUTION (Dr. R. Spindel and Dr. E. Weinstein, Library)	3
YALE UNIV. (Library, Prof. P. Schultheiss and Prof. F. Tuteur)	3